arXiv:1610.08367v1 [stat.ME] 26 Oct 2016

Nonparametric Dynamic State Space Modeling of Observed Circular Time Series with Circular Latent States: A Bayesian Perspective

Satyaki Mazumder[1] and Sourabh Bhattacharya[2]

[1]Indian Institute of Science Education and Research Kolkata
[2]Indian Statistical Institute, Kolkata.

Abstract

Circular time series has received relatively little attention in statistics and modeling complex circular time series using the state space approach is non-existent in the literature. In this article we introduce a flexible Bayesian nonparametric approach to state space modeling of observed circular time series where even the latent states are circular random variables. Crucially, we assume that the forms of both observational and evolutionary functions, both of which are circular in nature, are unknown and time-varying. We model these unknown circular functions by appropriate wrapped Gaussian processes having desirable properties.

We develop an effective Markov chain Monte Carlo strategy for implementing our Bayesian model, by judiciously combining Gibbs sampling and Metropolis-Hastings methods. Validation of our ideas with a simulation study and two real bivariate circular time series data sets, where we assume one of the variables to be unobserved, revealed very encouraging performance of our model and methods.

We finally analyse a data consisting of directions of whale migration, considering the unobserved ocean current direction as the latent circular process of interest. The results that we obtain are encouraging, and the posterior predictive distribution of the observed process correctly predicts the observed whale movement.

Keywords: *Circular time series; Latent circular process; Look-up table; Markov Chain Monte Carlo; State-space model; Wrapped Gaussian process.*

Contents

1 Introduction **3**

2 Dynamic state space model with circular latent and observed states **5**

2.1 Wrapped Gaussian process representations of the observational and evolutionary functions 6

2.2 Bayesian hierarchical structure of our proposed model 7

2.3 Prior specifications 7

3 MCMC-based inference **8**

4 Simulation study **11**

4.1 True model 11

4.2 Choices of prior parameters and the grid $\boldsymbol{G}_z$ 11

4.3 MCMC details 12

4.4 Results of simulation study 12

5 Model validation with real data analysis **13**

5.1 Wind pair data 15

5.1.1 Brief description of the data 15

5.1.2 Prior choices and MCMC implementations 15

5.1.3 Results 15

5.2 Spawning time and low tide time data 16

5.2.1 A brief description of the data set 16

5.2.2 Prior choices and MCMC implementations for spawning time data 18

5.3 Results and discussions on spawning time data 19

6 Application to whale positional data **22**

6.1 A brief description of the data set 22

6.2 Prior choices and MCMC implementation 22

6.3 Results of whale positional data 23

7 Discussion and conclusion **25**

S-1Full conditional distributions of $\boldsymbol{\beta}_f$ **29**

S-2 Full conditional distribution of σ_f **29**

S-3 Full conditional density of σ_ϵ **30**

S-4 Full conditional density of $\boldsymbol{f}^*_{D_T}$ **30**

S-5 Full conditional distribution of $f^*(T+1, x_{T+1})$ **30**

S-6 Full conditional density of N_t, $t = 1, \ldots, T$ **31**

S-7 Full conditional density of $\boldsymbol{\beta}_g$ **31**

S-8 Full conditional density of σ^2_η **32**

S-9 Full conditional density of σ^2_g **33**

S-10 Full conditional distribution of x_0 **33**

S-11 Full conditional density of $g^*(1, x_0)$ **33**

S-12 Full conditional of $\boldsymbol{D}_z$ **34**

S-13 Full conditional of x_1 **35**

S-14 Full conditional of x_{t+1}, for $t = 1, \ldots, T-1$ **35**

S-15 Full conditional of x_{T+1} **36**

S-16 Full conditional density of K_1 **36**

S-17 Full conditional density of K_t **36**

1 Introduction

In contrast with the traditional time series where the variables take values on the real line, circular time series with angular variables have received much less attention in the statistical literature. Some of the relatively scarce undertakings on circular time series, all in the classical statistical framework, are Breckling (1989), Fisher and Lee (1994), Holzmann *et al.* (2006), Hughes (2007) and Marzio *et al.* (2012). The classical approach, however, is limited to models with relatively simple dependence structures, such as p-th order Markov dependence, to enable inference. Far more flexible and realistic models can be accommodated within the Bayesian paradigm without any compromise; the inference can be carried out arbitrarily accurately using powerful Markov chain Monte Carlo (MCMC) methods. In this article, we propose and develop a novel and highly flexible approach to modeling circular time series using a Bayesian nonparametric state space approach, and an effective MCMC methodology for Bayesian inference.

Indeed, versatility of state space structures in modeling complex time series is well-appreciated in various scientific disciplines such as statistics, engineering, economics, biology, ecology, finance, and most of the existing time series models admit the state space representation. Notably, state space models consist of an observational equation for the observed part of the time series and an evolutionary equation that accounts for the latent, unobserved process that is presumed to affect the observed process. In this work, we shall concern ourselves with Bayesian state space modeling of complex circular time series data, where the latent process is also circular in nature, and where the observational and evolutionary functions are time-varying, but unknown. We model both the unknown functions nonparametrically using appropriate wrapped Gaussian process priors developed by Mazumder and Bhattacharya (2016a). For our state space model, the circular observations are conditionally independent given the latent states and the observational function, and the latent states have the Markov property conditionally on the evolutionary function. Unconditionally, however, the latent circular states are realizations of a complex, intractable stochastic process possessing a complex, intractable dependence structure in a way that all the latent states depend upon each other. The observed circular process is also intractable unconditionally, with a dependence structure that makes all the observational variables interdependent. However, the attractive properties of the wrapped Gaussian process prior ensure that the dependence structures, although complex, are very reasonable. Thus, our Bayesian state space modeling approach frees the circular time series paradigm of the limitations of the classical approach, while the MCMC procedure we propose, takes care of the inference part.

It is worth noting that Mazumder and Bhattacharya (2016a) developed a Bayesian nonparametric state space approach to modeling observed linear time series, assuming circular latent process. The obvious difference of our current work with theirs is that in our case, even the observed time series is circular. This circular extension of the observed process, however, is not insignificant, and throws much difficult challenges compared to the approach of Mazumder and Bhattacharya (2016a). In particular, because of our Gaussian process approach, the joint distribution of the observed data conditional on the latent states and the other parameters, is a product of wrapped normal distributions, for which closed forms are not available, and as many discrete auxiliary variables as the data size needed to be introduced to express the likelihood conditional on these auxiliary variables. To make things harder, these wrapped normal distributions, even conditionally on the auxiliary variables, involve the unknown observational function in a way that it can not be integrated out as in Mazumder and Bhattacharya (2016a). Indeed, thanks to the linear nature of the observed process, Mazumder and Bhattacharya (2016a) could marginalize over the unknown observational function to arrive at a multivariate normal distribution of the observed data conditionally on the latent states and other parameters.

Combination of our involved conditional distribution of the observed data with the heavily involved form of the joint distribution of the state variables yields a structure that is way beyond the scope of Mazumder and Bhattacharya (2016a). It is thus clear that in comparison with Mazumder and Bhattacharya (2016a), a substantially different and involved MCMC method is also required for the implementation of our approach.

Once we build the necessary Bayesian nonparametric model and methods, we evaluate them on a simulated data generated from a state space model with specific circular observational and circular evolutionary equations, but fitted with our proposed model and methods. We also consider two real data sets for validation of our ideas. In one case, wind directions at 6.00 am and 12.00 pm on each of 21 days, are recorded. Pretending that the wind directions at 6.00 am are unobserved, we obtain the posteriors of these circular latent states and compare it with the actual observed values. The second data set for our validation purpose consists of spawning time of a particular fish and the low tide times, both measured on the 24-hour clock, for 86 days. In this case, we assume that the low tide times are unobserved, and fit our Bayesian model, viewing the times as circular variables. In all the three cases, we obtained excellent predictions of the latent circular states and excellent forecasts of both latent and observed states.

We then apply our ideas to a real data set consisting of only the directions associated with movements of a whale in course of its migration. The directions of ocean current, which are presumed to influence the

movements of the whale, are not observed, and hence, we consider them to be the latent circular states of interest. Our Bayesian model and methods yielded quite sensible results on the latent states and correct prediction of the whale movement.

The rest of this article is structured as follows. In Section 2 we introduce our Bayesian state space model with circular observed data and circular latent states, discussing our wrapped Gaussian process prior and explicitly providing the form of the Bayesian hierarchical model, and the forms of the priors on the parameters. In Section 3 we briefly discuss the main technical issues distinguishing our MCMC method with that of Mazumder and Bhattacharya (2016a), showing that our present MCMC methodology is far more involved. The details of our MCMC procedure are provided in the supplement Mazumder and Bhattacharya (2016b). We then validate our model and methods with a simulation study in Section 4 and two real data sets on pairs of wind directions and spawning/low tide times in Section 5. We apply our ideas to the whale data in Section 6, obtaining the posteriors of the ocean current directions and forecasting whale movement. Finally, we summarize our work and provide concluding remarks in Section 7.

2 Dynamic state space model with circular latent and observed states

Our proposed state space model is as follows: For $t = 1, 2, \ldots T$,

$$y_t = \{f(t, x_t) + \epsilon_t\} \ [2\pi], \quad \epsilon_t \sim N(0, \sigma_\epsilon^2), \tag{1}$$

$$x_t = \{g(t, x_{t-1}) + \eta_t\} \ [2\pi], \quad \eta_t \sim N(0, \sigma_\eta^2), \tag{2}$$

where $\{y_t;\ t = 1, \ldots, T\}$ is the observed circular time series; $\{x_t;\ t = 0, 1, \ldots, T\}$ are the latent circular states; $f(\cdot, \cdot)$ and $g(\cdot, \cdot)$ are the unknown evolutionary functions with values on the circular manifold. In equations (1) and (2), $[2\pi]$ stands for the mod 2π operation. Note that

$$\{f(t, x_{t-1}) + \epsilon_t\} \ [2\pi] = \{f^*(t, x_{t-1}) + \epsilon_t\} \ [2\pi] \tag{3}$$

and

$$\{g(t, x_{t-1}) + \eta_t\} \ [2\pi] = \{g^*(t, x_{t-1}) + \eta_t\} \ [2\pi], \tag{4}$$

where f^* and g^* are the linear counterparts of f and g, that is, $f^*(t, x_{t-1})$ is the linear random variable such that $f^*(t, x_{t-1})\ [2\pi] = f(t, x_{t-1})$ and similarly, $g^*(t, x_{t-1})\ [2\pi] = g(t, x_{t-1})$. For convenience, we shall frequently use the representations (3) and (4). For more details on such a representation the reader is referred to Mazumder and Bhattacharya (2016a). Indeed, to derive the distributions of y_t and x_t, we shall first obtain the distributions of the linear random variables $f^*(t, x_{t-1}) + \epsilon_t$ and $g^*(t, x_{t-1}) + \eta_t$ and then apply the mod 2π operation to these variables to derive the distribution of the circular variables y_t and x_t.

Note that both the observational and evolutionary functions have the linear argument t and the angular argument x. The linear argument guarantees that the functions are time-varying, that is, the functions are allowed to freely evolve with time.

2.1 Wrapped Gaussian process representations of the observational and evolutionary functions

We now provide a brief discussion on modeling the unknown circular functions f and g. Mazumder and Bhattacharya (2016a) have constructed a wrapped Gaussian process by convolving a suitable kernel with standard Wiener process as a function of time and directions. The created wrapped Gaussian process has the desirable properties; for example, the covariance becomes 0 whenever the difference between the angles becomes $\pi/2$, implying orthogonality of the directions, irrespective of the value of the time difference. Similarly, as the time difference goes to ∞, the covariance converges to 0. Moreover, the desired continuity and smoothness properties do hold for the constructed Gaussian process (the proofs are provided in the supplement of Mazumder and Bhattacharya (2016a)). While constructing such a wrapped Gaussian process the basic idea was to first construct a Gaussian process as a function of time and angle and then apply the mod 2π operation. Here also, to model f and g, we first model f^* and g^*, the linear parts of f and g, using the Gaussian process, created in Mazumder and Bhattacharya (2016a). The mean functions of f^* and g^* are of the forms $\mu_f(\cdot, \cdot) = \boldsymbol{h}(\cdot, \cdot)'\boldsymbol{\beta}_f$ and $\mu_g(\cdot, \cdot) = \boldsymbol{h}(\cdot, \cdot)'\boldsymbol{\beta}_g$, where $\boldsymbol{h}(t, z) = (1, t, \cos(z), \sin(z))'$; here z is an angular quantity and $\boldsymbol{\beta}_f$, $\boldsymbol{\beta}_g$ are parameters in $\mathbb{R}^4$. For any fixed (t_1, z_1) and (t_2, z_2), where t_1, t_2 are linear quantities and z_1, z_2 are angular quantities, the covariance structures are given by $c_f((t_1, z_1), (t_2, z_2)) = \exp\{-\sigma_f^4(t_1 - t_2)^2\}\cos(|z_1 - z_2|)$ and $c_g((t_1, z_1), (t_2, z_2)) = \exp\{-\sigma_g^4(t_1 - t_2)^2\}\cos(|z_1 - z_2|)$, where σ_f and σ_g are positive, real valued parameters. For details, see Mazumder and Bhattacharya (2016a). After modeling f^* and g^* by the aforementioned Gaussian process, we derive the wrapped Gaussian distribution of $f(\cdot, \cdot) + \epsilon_t$ and $g(\cdot, \cdot) + \eta_t$ using the mod 2π operation on

the distributions of $f^*(\cdot,\cdot)+\epsilon_t$ and $g^*(\cdot,\cdot)+\eta_t$, respectively.

2.2 Bayesian hierarchical structure of our proposed model

Our modeling approach can be described succinctly by the following hierarchical Bayesian representation:

$$[y_t|f,\boldsymbol{\theta}_f,x_t] \sim N\left(f^*(t,x_t),\sigma^2_\epsilon\right)\ [2\pi];\ t=1,\ldots,T, \tag{5}$$

$$[x_t|g,\boldsymbol{\theta}_g,x_{t-1}] \sim N\left(g^*(t,x_{t-1}),\sigma^2_\eta\right)[2\pi];\ t=1,\ldots,T, \tag{6}$$

$$[x_0] \sim N\left(\mu_{x_0},\sigma^2_{x_0}\right)[2\pi], \tag{7}$$

$$[f(\cdot,\cdot)|\boldsymbol{\theta}_f] \sim GP\left(\boldsymbol{h}(\cdot,\cdot)'\boldsymbol{\beta}_f,\sigma^2_f c_f(\cdot,\cdot)\right)\ [2\pi], \tag{8}$$

$$[g(\cdot,\cdot)|\boldsymbol{\theta}_g] \sim GP\left(\boldsymbol{h}(\cdot,\cdot)'\boldsymbol{\beta}_g,\sigma^2_g c_g(\cdot,\cdot)\right)[2\pi], \tag{9}$$

$$[\boldsymbol{\beta}_f,\sigma^2_f,\boldsymbol{\beta}_g,\sigma^2_g,\sigma^2_\epsilon,\sigma^2_\eta] = [\boldsymbol{\beta}_f,\sigma^2_f][\boldsymbol{\beta}_g,\sigma^2_g][\sigma^2_\epsilon,\sigma^2_\eta], \tag{10}$$

where $\boldsymbol{\theta}_f=(\boldsymbol{\beta}_f,\sigma_f,\sigma_\epsilon)'$ and $\boldsymbol{\theta}_g=(\boldsymbol{\beta}_g,\sigma_g,\sigma_\eta)'$. In the above, GP stands for "Gaussian Process".

For obtaining the joint distribution of the latent circular state variables, we utilize the "look-up" table approach (see Bhattacharya (2007)) along the same line as Mazumder and Bhattacharya (2016a). The idea and the complete details of the look-up table approach in the context of circular latent variable is discussed in Mazumder and Bhattacharya (2016a), and thereby we skip the details in this current article. In the next section we provide the forms of the prior distributions of the parameters associated with the above hierarchical structure.

2.3 Prior specifications

Our prior distributions have the following forms.

$$[x_0] \sim \text{von Mises}(\mu_0,\sigma^2_0) \tag{11}$$

$$[\sigma^2_\epsilon] \propto (\sigma^2_\epsilon)^{\left(-\frac{\alpha_\epsilon+2}{2}\right)}\ \exp\ \left\{-\frac{\gamma_\epsilon}{2\sigma^2_\epsilon}\right\};\quad \alpha_\epsilon,\ \gamma_\epsilon>0 \tag{12}$$

$$[\sigma^2_\eta] \propto (\sigma^2_\eta)^{\left(-\frac{\alpha_\eta+2}{2}\right)}\ \exp\ \left\{-\frac{\gamma_\eta}{2\sigma^2_\eta}\right\};\quad \alpha_\eta,\ \gamma_\eta>0 \tag{13}$$

$$[\sigma^2_g] \propto (\sigma^2_g)^{\left(-\frac{\alpha_g+2}{2}\right)}\ \exp\ \left\{-\frac{\gamma_g}{2\sigma^2_g}\right\};\quad \alpha_g,\ \gamma_g>0 \tag{14}$$

$$[\sigma_f^2] \propto (\sigma_f^2)^{\left(-\frac{\alpha_f+2}{2}\right)} \exp\left\{-\frac{\gamma_f}{2\sigma_f^2}\right\}; \quad \alpha_f,\, \gamma_f > 0 \tag{15}$$

$$[\boldsymbol{\beta}_f] \sim N_4(\boldsymbol{\beta}_{f,0}, \Sigma_{\beta_{f,0}}); \tag{16}$$

$$[\boldsymbol{\beta}_g] \sim N_4(\boldsymbol{\beta}_{g,0}, \Sigma_{\beta_{g,0}}). \tag{17}$$

Here, by $N_4(\cdot,\cdot)$, we mean the 4 variate normal distribution. We discuss the choice of prior parameters in Sections 4, 5 and 6, in the contexts of applications to simulated and real data sets.

3 MCMC-based inference

The aim of our MCMC-based inference is to address the problem of forecasting y_{T+1} and to learn about the latent circular states, given the observed data set $\boldsymbol{D}_T = (y_1, \ldots, y_T)'$. Unlike Mazumder and Bhattacharya (2016a) here y_t is circular and hence dealing with the conditional distribution of y_{T+1} given the data $\boldsymbol{D}_T$ is rendered far more difficult. As already remarked in Section 1, the distribution of the observed variables is circular normal, and does not admit any closed form expression. To deal with such a situation one needs to bring in the auxiliary variables $N_t = \langle y_t^*/2\pi \rangle$, where y_t^* is the linear part of the circular variable y_t and $\langle u \rangle$ denotes the largest integer not exceeding u. The wrapped random variable N_t can take values in the set $\mathbb{Z}$, where $\mathbb{Z}$ denotes the set of the integers. For details on wrapped variable in the context of circular data, see, for example, Ravindran and Ghosh (2011); see also Mazumder and Bhattacharya (2016a). However, even conditionally on the auxiliary variables, f^* can not be marginalized out of the model to simplify the proceedings, so that our MCMC method must include simulation of f^*, in addition to the auxiliary variables. In contrast, Mazumder and Bhattacharya (2016a) was able to work with a much simpler form thanks to joint conditional normality of their linear observed data, which also enabled them to integrate out the unknown observational function, further simplifying their proceedings.

In our case, the posterior distribution of y_{T+1} given $\boldsymbol{D}_T$ by introducing auxiliary variables $N_1, \ldots, N_T$ admits the following form:

$$\begin{aligned}
&[y_{T+1}|\boldsymbol{D}_T] \\
&= \sum_{N_1,\ldots,N_T} \int \big[y_{T+1}|\boldsymbol{D}_T, f^*(1,x_1), \ldots, f^*(T+1, x_{T+1}), N_1, \ldots N_T, x_0, \ldots, x_{T+1}, \boldsymbol{\beta}_f, \boldsymbol{\beta}_g, \sigma_f,
\end{aligned}$$

$$\sigma_g, \sigma_\epsilon, \sigma_\eta] \, [f^*(1, x_1), \ldots, f^*(T+1, x_{T+1}), N_1, \ldots N_T, x_0, \ldots, x_{T+1}, \boldsymbol{\beta}_f, \boldsymbol{\beta}_g, \sigma_f, \sigma_g, \sigma_\epsilon, \sigma_\eta | \boldsymbol{D}_T]$$

$$df^*(1, x_1) \ldots df^*(T+1, x_{T+1}) dx_0 \ldots dx_{T+1} d\boldsymbol{\beta}_f d\boldsymbol{\beta}_g d\sigma_f d\sigma_g d\sigma_\epsilon d\sigma_\eta. \tag{18}$$

Therefore, once we have a sample from the joint posterior $[f^*(1, x_1), \ldots, f^*(T+1, x_{T+1}), N_1, \ldots, N_T, x_0, \ldots, x_{T+1}, \boldsymbol{\beta}_f, \boldsymbol{\beta}_g, \sigma_f, \sigma_g, \sigma_\epsilon, \sigma_\eta | \boldsymbol{D}_T]$, we can generate an observation from $[y_{T+1} | \boldsymbol{D}_T]$ by simply generating an observation from $[y_{T+1} | \boldsymbol{D}_T, f^*(1, x_1), \ldots, f^*(T+1, x_{T+1}), N_1, \ldots N_T, x_0, \ldots, x_{T+1}, \boldsymbol{\beta}_f, \boldsymbol{\beta}_g, \sigma_f, \sigma_g, \sigma_\epsilon, \sigma_\eta]$. Further, we note that given a sample from $[f^*(1, x_1), \ldots, f^*(T+1, x_{T+1}), N_1, \ldots N_T, x_0, \ldots, x_{T+1}, \boldsymbol{\beta}_f, \boldsymbol{\beta}_g, \sigma_f, \sigma_g, \sigma_\epsilon, \sigma_\eta$ $\boldsymbol{D}_T]$, y_{T+1} has a wrapped normal distribution with parameter $f^*(T+1, x_{T+1})$ and σ_ϵ^2, because

$$[y_{T+1} | \boldsymbol{D}_T, f^*(1, x_1), \ldots, f^*(T+1, x_{T+1}), N_1, \ldots N_T, x_0, \ldots, x_{T+1}, \boldsymbol{\beta}_f, \boldsymbol{\beta}_g, \sigma_f, \sigma_g, \sigma_\epsilon, \sigma_\eta]$$

$$= [y_{T+1} | f^*(T+1, x_{T+1}), \sigma_\epsilon, x_{T+1}].$$

Therefore, we need to obtain a sample from $[f^*(1, x_1), \ldots, f^*(T+1, x_{T+1}), N_1, \ldots N_T, x_0, \ldots, x_{T+1}, \boldsymbol{\beta}_f, \boldsymbol{\beta}_g, \sigma_f, \sigma_g, \sigma_\epsilon, \sigma_\eta | \boldsymbol{D}_T]$. Define $\boldsymbol{f}^* = (f^*(1, x_1), \ldots, f^*(T+1, x_{T+1}))' = (\boldsymbol{f}^*_{D_T}, f^*(T+1, x_{T+1}))'$. Note that given $(x_1, \ldots, x_{T+1})', \boldsymbol{\beta}_f$, and σ_f, $\boldsymbol{f}^*$ follows a $(T+1)$-multivariate normal distribution with mean $E\left[\boldsymbol{f}^* | (x_1, \ldots, x_{T+1})', \boldsymbol{\beta}_f\right] = H\boldsymbol{\beta}_f$, and covariance matrix $\sigma_f^2 \boldsymbol{A}_f$, where $H = [\boldsymbol{h}'(1, x_1) \cdots \boldsymbol{h}'(T+1, x_{T+1})]'$ and $\boldsymbol{A}_f = (\exp\left(-\sigma_f^4 (i-j)^2\right) \cos(|x_i - x_j|);\ 1 \le i, j \le (T+1))$. Therefore, $\boldsymbol{f}^*_{D_T}$ given $(x_1, \ldots, x_T)', \boldsymbol{\beta}_f$ and σ_f, follows a T-variate normal with mean $H_{D_T}\boldsymbol{\beta}_f$ and covariance $\boldsymbol{A}_{f,D_T}$, where $H_{D_T} = [\boldsymbol{h}'(1, x_1) \cdots \boldsymbol{h}'(T, x_T)]'$ and $\boldsymbol{A}_{f,D_T} = (\exp\left(-\sigma_f^4 (i-j)^2\right) \cos(|x_i - x_j|);\ 1 \le i, j \le T)$. Moreover, it is immediate that $[f^*(T+1, x_{T+1}) | \boldsymbol{f}^*_{D_T}, x_{T+1}, \boldsymbol{\beta}_f, \sigma_f] \sim N(\mu_{f^*(T+1, x_{T+1})}, \sigma^2_{f^*(T+1, x_{T+1})})$, where $\mu_{f^*(T+1, x_{T+1})} = \boldsymbol{h}'(T+1, x_{T+1})\boldsymbol{\beta}_f + s_{f,D_T}(T+1, x_{T+1})' \boldsymbol{A}^{-1}_{f,D_T} (\boldsymbol{f}^*_{D_T} - H_{D_T}\boldsymbol{\beta}_f)$ and $\sigma^2_{f^*(T+1, x_{T+1})} = \sigma_f^2 (1 - s_{f,D_T}(T+1, x_{T+1})' \boldsymbol{A}^{-1}_{f,D_T} s_{f,D_T}(T+1, x_{T+1}))$ with

$$s_{f,D_T}(T+1, x_{T+1})' = (\exp(-\sigma_f^4 (T+1-j)^2) \cos(|x_{T+1} - x_j|), 1 \le j \le T).$$

Now, by introducing the auxiliary variables $K_1, \ldots, K_T$, the wrapped variables for latent circular variables x_t, defined as $K_t = \langle x_t^* / 2\pi \rangle$, and the set of linear-circular grid points $\boldsymbol{D}_z$ (defined below), we can write

$$[\boldsymbol{f}^*, N_1 \ldots, N_T, x_0, \ldots, x_{T+1}, \boldsymbol{\beta}_f, \boldsymbol{\beta}_g, \sigma_f, \sigma_g, \sigma_\epsilon, \sigma_\eta | \boldsymbol{D}_T]$$

$$\propto \sum_{K_1, \ldots, K_T} \int [\boldsymbol{f}^*, N_1 \ldots, N_T, x_0, \ldots, x_{T+1}, \boldsymbol{\beta}_f, \boldsymbol{\beta}_g, \sigma_f, \sigma_g, \sigma_\epsilon, \sigma_\eta, g^*(1, x_0), \boldsymbol{D}_z, \boldsymbol{D}_T] dg^* d\boldsymbol{D}_z$$

$$= \sum_{K_1,\ldots,K_T} \int [\boldsymbol{\beta}_f][\boldsymbol{\beta}_g][\sigma_f][\sigma_g][\sigma_\epsilon][\sigma_\eta][x_0][\boldsymbol{f}^*_{D_T}|x_1,\ldots,x_T,\boldsymbol{\beta}_f,\sigma_f][f^*(T+1,x_{T+1})|\boldsymbol{f}^*_{D_T},x_{T+1},\boldsymbol{\beta}_f,\sigma_f]$$
$$\times \prod_{t=1}^{T}[N_t|f^*(t,x_t),\sigma_\epsilon,x_t][g^*(1,x_0)|x_0,\boldsymbol{\beta}_g,\sigma_g][\boldsymbol{D}_z|g^*(1,x_0),x_0,\boldsymbol{\beta}_g,\sigma_g][x_1|g^*(1,x_0),\sigma_\eta,K_1][K_1|g^*(1,x_0),\sigma_\eta]$$
$$\times \prod_{t=2}^{T+1}[x_t|\boldsymbol{\beta}_g,\sigma_\eta,\sigma_g,\boldsymbol{D}_z,x_{t-1},K_t]\prod_{t=2}^{T+1}[K_t|\boldsymbol{\beta}_g,\sigma_\eta,\sigma_g,\boldsymbol{D}_z,x_{t-1}]\,[\boldsymbol{D}_T|x_1,\ldots,x_T,f^*(1,x_1),\ldots,f^*(T,x_T),$$
$$N_1,\ldots,N_T,\sigma_\epsilon]\,d\boldsymbol{D}_z dg^*(1,x_0). \tag{19}$$

We note that $[\boldsymbol{D}_T|x_1,\ldots,x_T,f^*(1,x_1),\ldots,f^*(T,x_T),N_1,\ldots,N_T,\sigma_\epsilon] = \prod_{t=1}^{T}[y_t|N_t,f^*(t,x_t),\sigma_\epsilon,x_t]$, and $\boldsymbol{D}_z = (g^*(t_1,z_1),\ldots,g^*(t_n,z_n))'$, where, for $i=1,\ldots,n$, (t_i,z_i) is a set of linear-circular grid-points with $t_i \geq 0$ and $z_i \in [0,2\pi]$, for $i=1,\ldots,n$. This grid, which we denote by $\boldsymbol{G}_z$, is associated with the look-up table; see Mazumder and Bhattacharya (2016a) for details. Hence, from (19), we obtain

$$[\boldsymbol{f}^*,N_1\ldots,N_T,x_0,\ldots,x_{T+1},\boldsymbol{\beta}_f,\boldsymbol{\beta}_g,\sigma_f,\sigma_g,\sigma_\epsilon,\sigma_\eta|\boldsymbol{D}_T]$$
$$\propto \sum_{K_1,\ldots,K_T} \int [\boldsymbol{\beta}_f][\boldsymbol{\beta}_g][\sigma_f][\sigma_g][\sigma_\epsilon][\sigma_\eta][x_0][\boldsymbol{f}^*_{D_T}|x_1,\ldots,x_T,\boldsymbol{\beta}_f,\sigma_f][f^*(T+1,x_{T+1})|\boldsymbol{f}^*_{D_T},x_{T+1},\boldsymbol{\beta}_f,\sigma_f]$$
$$\times \prod_{t=1}^{T}[N_t|f^*(t,x_t),\sigma_\epsilon,x_t][g^*(1,x_0|x_0,\boldsymbol{\beta}_g,\sigma_g)][\boldsymbol{D}_z|g^*(1,x_0),x_0,\boldsymbol{\beta}_g,\sigma_g][x_1|g^*(1,x_0),\sigma_\eta,K_1][K_1|g^*(1,x_0),\sigma_\eta]$$
$$\times \prod_{t=2}^{T+1}[x_t|\boldsymbol{\beta}_g,\sigma_\eta,\sigma_g,\boldsymbol{D}_z,x_{t-1},K_t]\prod_{t=2}^{T+1}[K_t|\boldsymbol{\beta}_g,\sigma_\eta,\sigma_g,\boldsymbol{D}_z,x_{t-1}]\prod_{t=1}^{T}[y_t|N_t,f^*(t,x_t),\sigma_\epsilon,x_t]d\boldsymbol{D}_z dg^*(1,x_0). \tag{20}$$

In (19) and (20) the identity $[\boldsymbol{f}^*|x_1,\ldots,x_{T+1},\boldsymbol{\beta}_f,\sigma_f] = \left[\boldsymbol{f}^*_{D_T}|x_1,\ldots,x_T,\boldsymbol{\beta}_f,\sigma_f\right]$
$\left[f^*(T+1,x_{T+1})|\boldsymbol{f}^*_{D_T},x_{T+1},\boldsymbol{\beta}_f,\sigma_f\right]$ is used.

The complete details of our MCMC algorithm is presented in the supplement.

4 Simulation study

4.1 True model

We now illustrate the performance of our model and methodologies using a simulation study, considering the following dynamic nonlinear model:

$$y_t = \{-\tan(\theta_t) + \tan^2(\theta_t)/20 + v_t\} \ [2\pi];$$
$$x_t = \left\{\alpha x_{t-1} + \frac{\beta x_{t-1}}{1+x_{t-1}^2} + \gamma \cos(1.2(t-2)) + u_t\right\} \ [2\pi],$$

for $t = 1, \ldots, T$ with $T = 101$. In the above, u_t and v_t are normally distributed with means zero and variances σ_η^2 and σ_ϵ^2. We choose the values of α, β and γ to be 1, 0.5 and 0.2, respectively, and fix the values of both σ_η and σ_ϵ at 0.1. The first 100 observations of y_t are assumed to be known, and the last observation is set aside for the purpose of forecasting.

4.2 Choices of prior parameters and the grid $\boldsymbol{G}_z$

For this simulation experiment we have chosen four variate normal prior distribution for $\boldsymbol{\beta}_f$ with mean $(0,0,0,0)'$ and covariance matrix as 4×4 identity matrix. The prior mean for $\boldsymbol{\beta}_g$ is taken to be $(1,1,1,1)'$. The choice of these prior parameters facilitated adequate mixing of our MCMC algorithm. As in Mazumder and Bhattacharya (2016a), we throughout fixed the third and fourth components of $\boldsymbol{\beta}_g$ to be 1 to tackle identifiability problems. Hence, we take the covariance matrix in the prior distribution of $\boldsymbol{\beta}_g$ as diagonal matrix with diagonal elements $(1,1,0,0)$.

Like Mazumder and Bhattacharya (2016a), in our current paper impropriety of the posteriors of σ_f, σ_ϵ, σ_g, σ_η, $K_t,\ t = 1, \ldots, T$ and $N_t,\ t = 1 \ldots, T$ result when they all permitted to be random. To be precise, for any value of N_t (or K_t), exactly the same of circular variable y_t (or x_t) is obtained by the mod 2π transformation applied to $y_t^* = y_t + 2\pi N_t$ (or $x_t^* = x_t + 2\pi K_t$). Therefore, given y_t (or x_t), it is not possible to constrain N_t (or K_t) unless both σ_f and σ_ϵ (or σ_g and σ_η) are bounded. Boundedness of σ_ϵ and σ_f (or σ_g and σ_η) would ensure finite variance of y_t (or x_t), which in turn would imply finite variability of N_t (or K_t). Since it is not immediate how to select a bounded prior for σ_f, σ_ϵ, σ_g and σ_η we obtain the maximum likelihood estimates (MLEs) of these variances and plug those values in our model. For obtaining the MLEs we used the simulated annealing technique (see, for instance, Robert and Casella (2004), Liu (2001)) where

at each iteration new values of these variances are considered, then all the other parameters are integrated out using average of Monte Carlo simulations, given the proposed values of σ_f, σ_ϵ, σ_g and σ_η, so that the integrated likelihood is obtained given the proposed variances. Then we calculated the acceptance ratio, and finally decreased the temperature parameter of our simulated annealing algorithm before proceeding to the next iteration. The values of the MLEs turned out to be $\hat{\sigma}_f = 2.64410$, $\hat{\sigma}_\epsilon = 0.29289$, $\hat{\sigma}_g = 0.20363$ and $\hat{\sigma}_\eta = 0.64201$.

Lastly, we divide the interval $[0, 2\pi]$ into 100 sub-intervals of the forms $\left[\frac{2\pi i}{100}, \frac{2\pi(i+1)}{100}\right]$, $i = 0, \ldots, 99$, and choose a random number uniformly for each of the sub-intervals; these values constitute the circular second component of the two dimensional grid $\boldsymbol{G}_z$. For the linear first component of $\boldsymbol{G}_z$, we choose a random number uniformly from each of the 100 subintervals $[i, i+1]$, $i = 0, \ldots, 99$.

4.3 MCMC details

Our MCMC algorithm updates some parameters using Gibbs steps and the remaining ones using Metropolis-Hastings steps; see the supplement for details. We update x_0 using von-Mises distribution with $\kappa = 3$, and for updating x_t we use a mixture of two von-Mises distributions with $\kappa = 0.5$ and $\kappa = 3$ for $t = 1, \ldots, T$. The wrapping variables N_t; $t = 1, \ldots T$ and K_t; $t = 1, \ldots, T$, are updated using the discrete normal random walk. The variance for normal distribution is taken to be 1. All these choices are made very painstakingly after cautiously adjudging the mixing properties of many pilot MCMC runs. The remaining parameters are updated using Gibbs steps.

We performed $2,50,000$ MCMC iterations with a burn-in period consisting of the first $2,00,000$ iterations using the above choices of the prior parameters and $\boldsymbol{G}_z$, and with the above MCMC updating procedure of the parameters. The time taken to run $2,50,000$ MCMC simulations in a server machine (64 bit, 1247.265 MHz CPU speed and 65 GB memory) is 25 hours and 34 minutes. The usual tests for convergence of MCMC iterations are performed and all the tests turned out to be satisfactory.

4.4 Results of simulation study

Figures 1 and 2 depict the posterior densities of the four components of $\boldsymbol{\beta}_f$ and the first two components of $\boldsymbol{\beta}_g$, respectively. The posterior predictive densities of x_{101} and y_{101} are provided in Figure 3. The horizontal bold black lines denote the 95% highest posterior density credible intervals and the vertical lines denote the true values. We observe that the true values of y_{101} and x_{101} fall well within the respective

intervals.

It is seen that the densities of most of x_t, $t = 1, \ldots, T$, have multiple modes. So, a plot of the posterior probability distribution of the latent process for each time point is more appropriate than ordinary credible regions. Such a plot for the latent circular time series $x_1, \ldots, x_T$ is displayed in Figure 4. In this plot, regions with progressively higher densities are shown by progressively more intense colors. Encouragingly, most of the true values are seen to lie in the high probability regions.

Thus, in nutshell, we can claim that our model performs quite optimistically, in spite of the true model being highly non-linear and assumed to be unknown. As a consequence, we expect our model and methods to perform adequately in general situations.

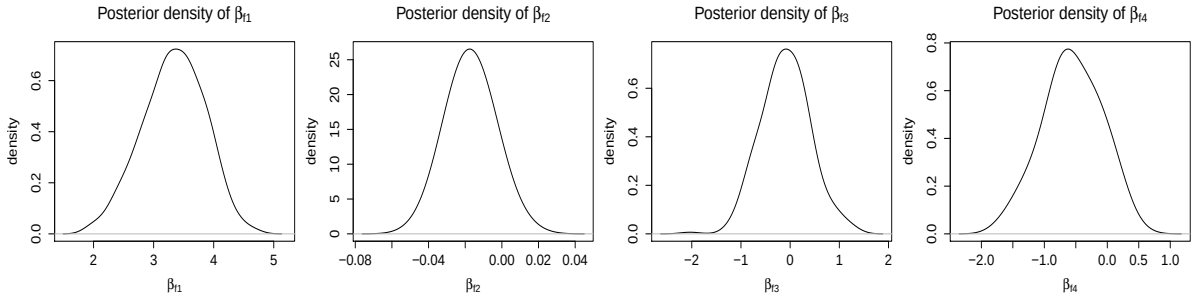

Figure 1: Posterior densities of the four components of $\boldsymbol{\beta}_f$ for simulated data.

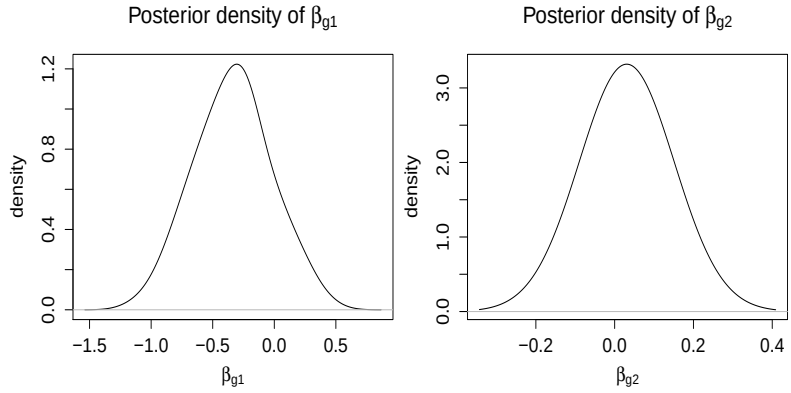

Figure 2: Posterior densities of the first and second components of $\boldsymbol{\beta}_g$ for simulated data.

5 Model validation with real data analysis

In this section we validate our methodologies by applying them to two circular time series data where the time-varying and circular covariates are originally known but we assume to be unknown. In other words, we attempt to predict the circular covariates considering them to be unobserved latent variables.

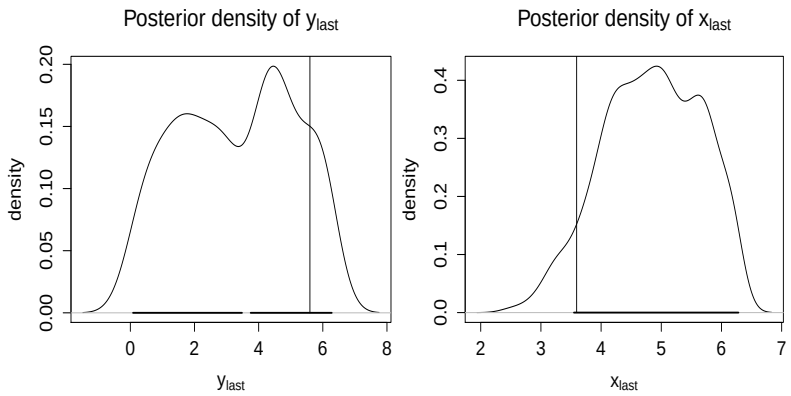

Figure 3: From left: The first panel displays the posterior predictive density of y_{101} of simulated data. The second plot represents the posterior predictive density of x_{101} (last latent observation). The thick horizontal line denotes the 95% highest posterior density credible interval and the vertical line denotes the true value for both the figures.

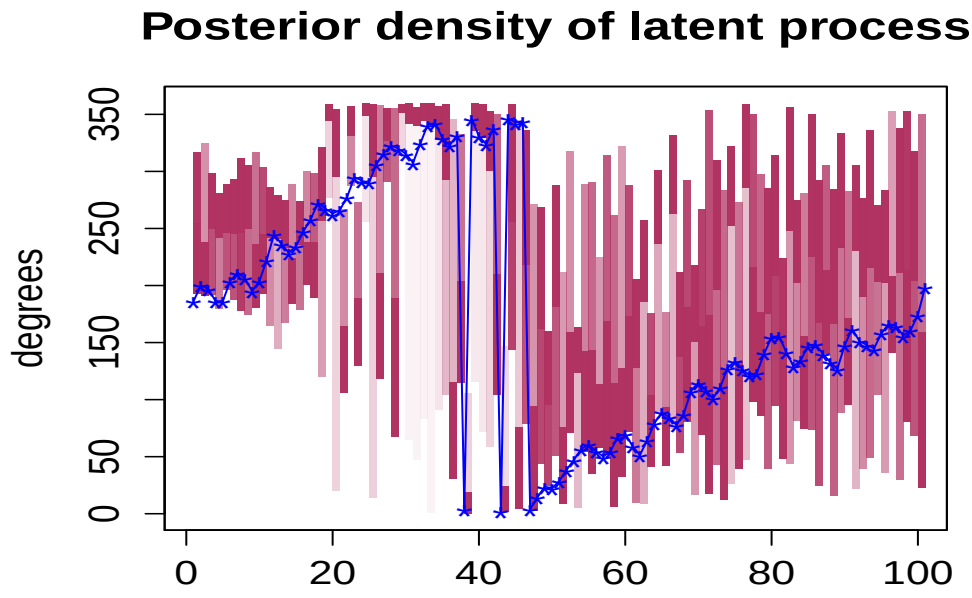

Figure 4: Depiction of the posterior densities of the latent circular process $\{x_t; t = 1, \ldots, T\}$; higher the intensity of the color, higher is the posterior density. The blue stars denote the true time series.

5.1 Wind pair data

5.1.1 Brief description of the data

Our first data set consists of a pair of wind directions recorded at 6.00 am and 12.00 noon for each of twenty one consecutive days at a weather station in Milwaukee. This data set, which is taken from Fisher (1993) (see page 253 of Fisher (1993) for more details of the data), is originally recorded in degrees; for our convenience, we converted them to radians ranging from 0 to 2π. Here we consider the wind directions at 6.00 am to be the latent circular variables and those at 12.00 noon, to be the observed variables. Moreover, we use 20 observations for our analysis and set aside last observation for the purpose of forecasting. In this study we are mainly interested in demonstrating how well our model is able to capture the recorded, real, wind direction data observed at 6.00 am, considered to be latent relative to our model. Plots of the true wind directions at both the time points for 21 days are provided in Figure 5.

5.1.2 Prior choices and MCMC implementations

We choose the prior means of $\boldsymbol{\beta}_f$ and $\boldsymbol{\beta}_g$ to be $(0,0,0,0)'$ and $(1,1,1,1)'$, respectively. As regards the prior covariance matrices of $\boldsymbol{\beta}_f$ and $\boldsymbol{\beta}_g$, we consider the identity matrix of dimension 4 and a diagonal matrix with diagonal entries as $(1,1,0,0)'$, respectively. To avoid identifiability issues, we fix the last two components of $\boldsymbol{\beta}_g$ at 1. The MLEs of σ_f, σ_ϵ, σ_g and σ_η, which are calculated using simulated annealing and assumed to be known thereafter, turned out to be 2.74891, 0.30649, 0.71260 and 0.36719, respectively. Using these prior parameters we run $3,50,000$ MCMC iterations and store the last $50,000$ observations for inference, discarding the first $3,00,000$ as burn in. The time taken by our server machine to implement 3,50,000 iterations of our MCMC algorithm is 11 hours 47 minutes.

5.1.3 Results

The posterior densities of the four components of the vector $\boldsymbol{\beta}_f$ and the two components of $\boldsymbol{\beta}_g$ are provided in Figures 6 and 7, respectively, and the posterior predictive densities of y_{21} and x_{21} are displayed in Figure 9. It is observed that the true values of y_{21} and x_{21} fall well within the 95% highest posterior density credible intervals, clearly demonstrating how well our model and the prior distributions of the parameters successfully describe the uncertainty present in the data (see, for instance, Box and Tiao (1973) and Bickel and Doksum (2007)). The marginal posterior densities of the latent variables are shown in Figure 8, where progressively higher intensities of the color denote regions of progressively higher posterior densities. The

blue stars in Figure 8 denote the true values of the wind directions at time 6.00 am. It is noted that the true values of the latent variable, namely, the wind directions at time 6.00 am (in radians), fall mostly in the respective high probability regions. Our Bayesian model and methods are particularly impressive in the sense that the highly nonlinear trend of the latent variable is adequately captured even when the data size is only 20. Since our nonparametric ideas permits the unknown observational and evolutionary function, based on Gaussian processes, to change with time, such encouraging performance is perhaps not surprising.

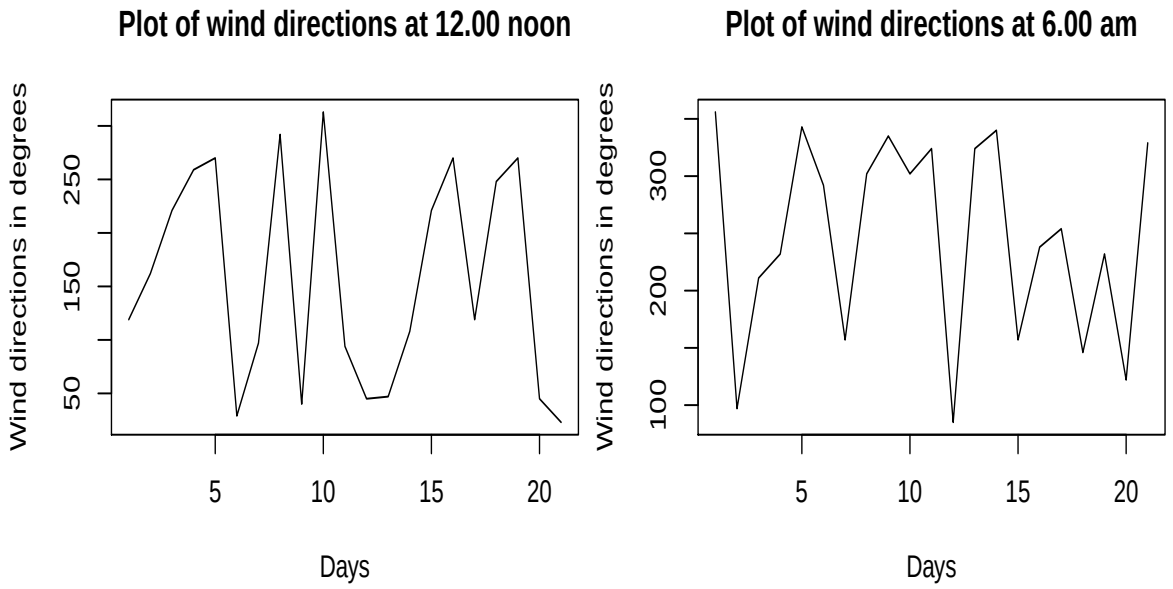
Plot of wind directions at 12.00 noon
Plot of wind directions at 6.00 am
Wind directions in degrees
Wind directions in degrees
Days
Days

Figure 5: Plot of the wind directions at 12.00 noon and 6.00 am for 21 days.

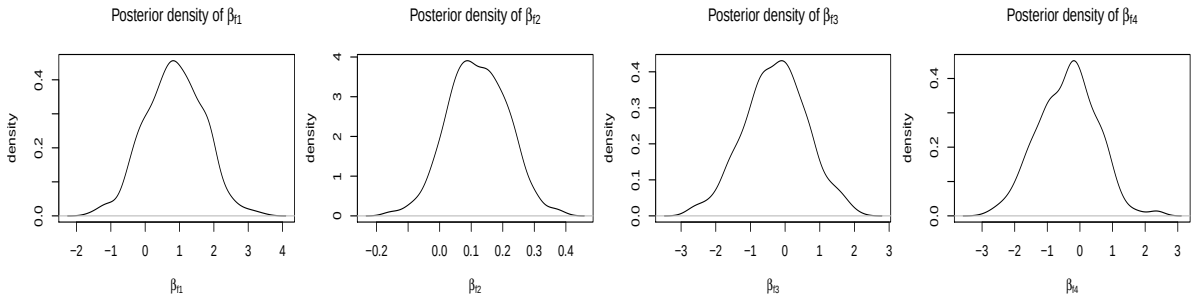

Figure 6: Posterior densities of the four components of $\boldsymbol{\beta}_f$ for the wind pair data.

5.2 Spawning time and low tide time data

5.2.1 A brief description of the data set

We apply our model and methodology to another real data set for the purpose of validation. Robert R. Warner at the University of California collected data on the spawning times of a particular fish in a

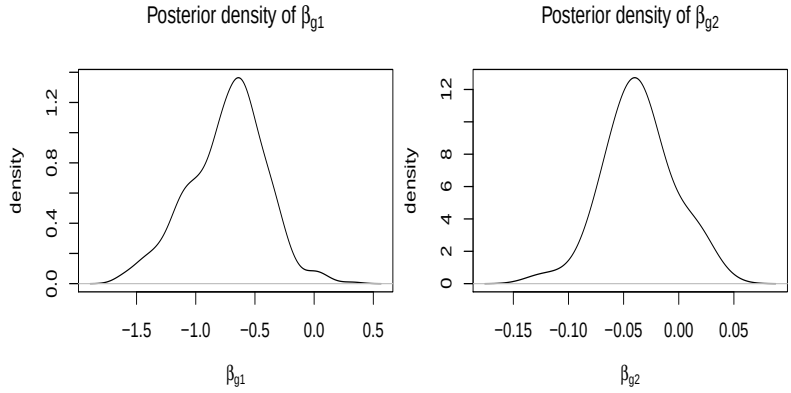

Figure 7: Posterior densities of the first two components of $\boldsymbol{\beta}_g$ for the wind pair data.

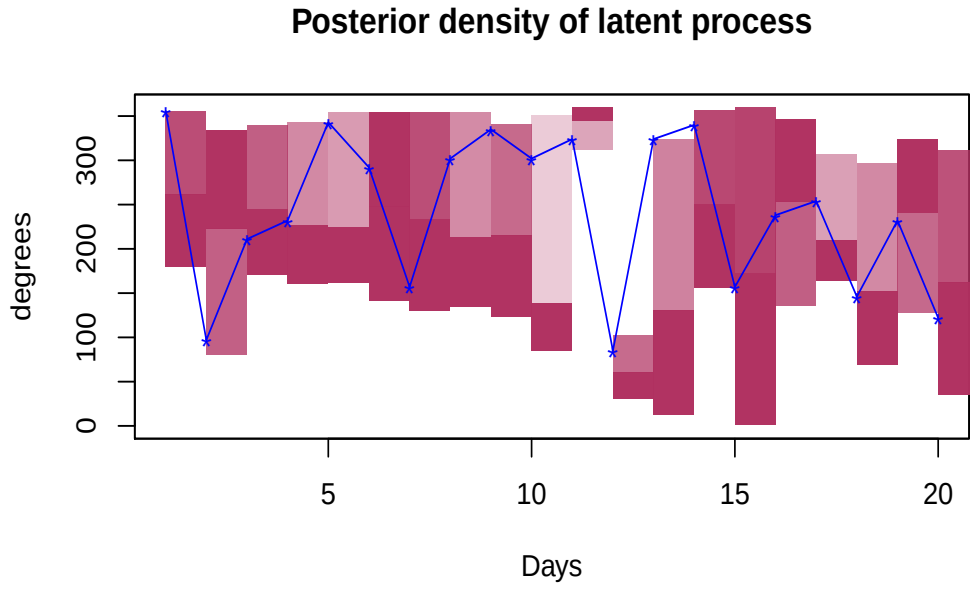

Figure 8: Representation of the marginal posterior densities of the latent variables corresponding to wind directions at 6.00 am as a color plot; progressively higher densities are represented by progressively intense colors. The blue stars represent the true wind directions (at 6.00 am) data.

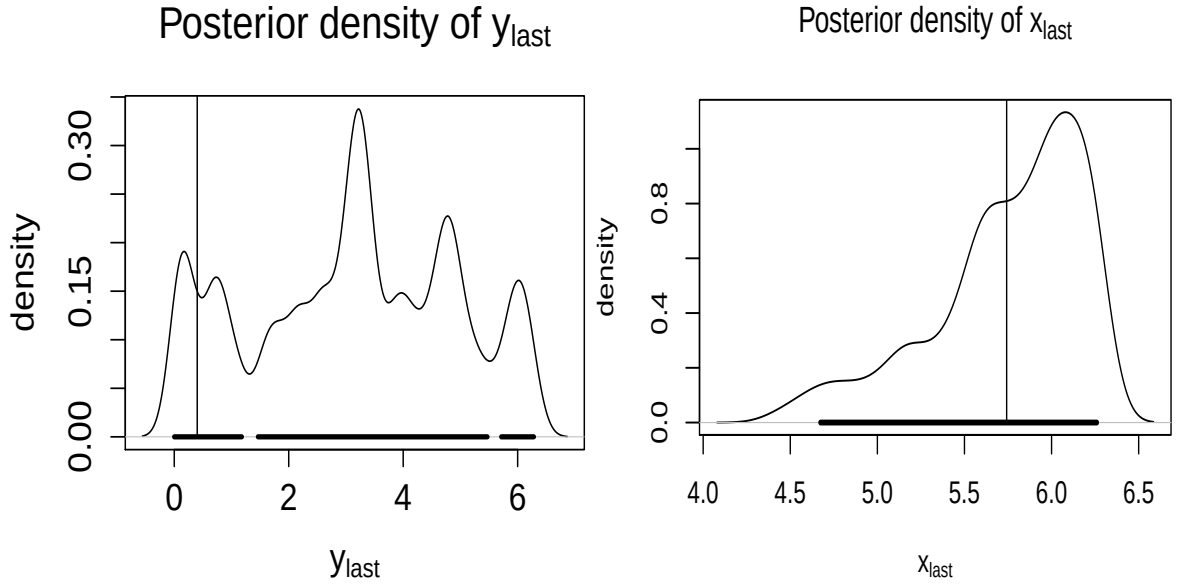

Figure 9: From left: The first panel displays the posterior predictive density of the 21st observation of wind directions at 12.00 noon for the wind pair data. The second plot represents the posterior predictive density of the 21st observation of wind direction at 6.00 am (latent variable). The thick horizontal line denotes the 95% highest posterior density credible interval and the vertical line denotes the true value (in radian) for both the panels.

marine biology study (see Lund (1999)). It is seen that the spawning time of a fish is influenced by the tidal characteristic of the fish's local environment. A regression study was done by Lund (1999) considering spawning time as dependent variable and time of low tide as the covariate. There are 86 observations for spawning times and low tide times. The plots of both the variables on the 24-hour clock scale are provided in Figure 10. We wrap the spawning time points and low tide time points on the $[0, 2\pi]$ scale (a corresponding plot is given in Figure 11) for our analysis. For our model we assume that the low tide times are latent and spawning times are observed. We use 85 observations for our analysis and set aside the last observation for the prediction purpose. As in Section 5.1 here also our main aim is to show that our methodology is equipped enough to capture the recorded low tide times, considered to be latent with respect to our model.

5.2.2 Prior choices and MCMC implementations for spawning time data

We choose the prior means of $\boldsymbol{\beta}_f$ and $\boldsymbol{\beta}_g$ to be $(0, 0, 0, 0)'$ and $(0, 1.25, 1, 1)'$, and the prior covariance matrices for $\boldsymbol{\beta}_f$ and $\boldsymbol{\beta}_g$ to be the identity matrix of dimension 4 and a diagonal matrix with diagonal entries as $(1, 1, 0, 0)'$, respectively, the latter matrix signifying, as usual, our attempt to resolve identifiability problems. The MLEs of σ_f, σ_ϵ, σ_g and σ_η, obtained by simulated annealing, turned out to be 1.97462, 0.37569, 0.67960 and 0.31686, respectively. We implemented $2,50,000$ iterations of our MCMC algorithm,

storing the last $50,000$ observations for inference. The time taken by our server machine to implement this exercise is 18 hours 54 minutes.

5.3 Results and discussions on spawning time data

We provide the plots of the posterior densities of the four components of $\boldsymbol{\beta}_f$ for the spawning time data in Figure 12 and those of the two components of $\boldsymbol{\beta}_g$ are displayed in Figure 13. The posterior densities of the latent variables, that is, low tide times, are depicted in Figure 14. As in the previous experiment, here also it is seen that the posterior densities of the latent variables are highly multimodal. The plots of the posterior densities of the latent process for all the time points are presented in Figure 14, where the observed values of the low tide times are denoted by the blue colored stars. Encouragingly, all the true values, except only the first three points, fall in the high probability density regions. Finally the posterior predictive densities of x_{86} and y_{86}, displayed in Figure 15, show that the true values of x_{86} and y_{86} fall well within the 95% highest posterior probability density region. We have conducted usual tests of MCMC convergence diagnosis, all of which turned out to be satisfactory.

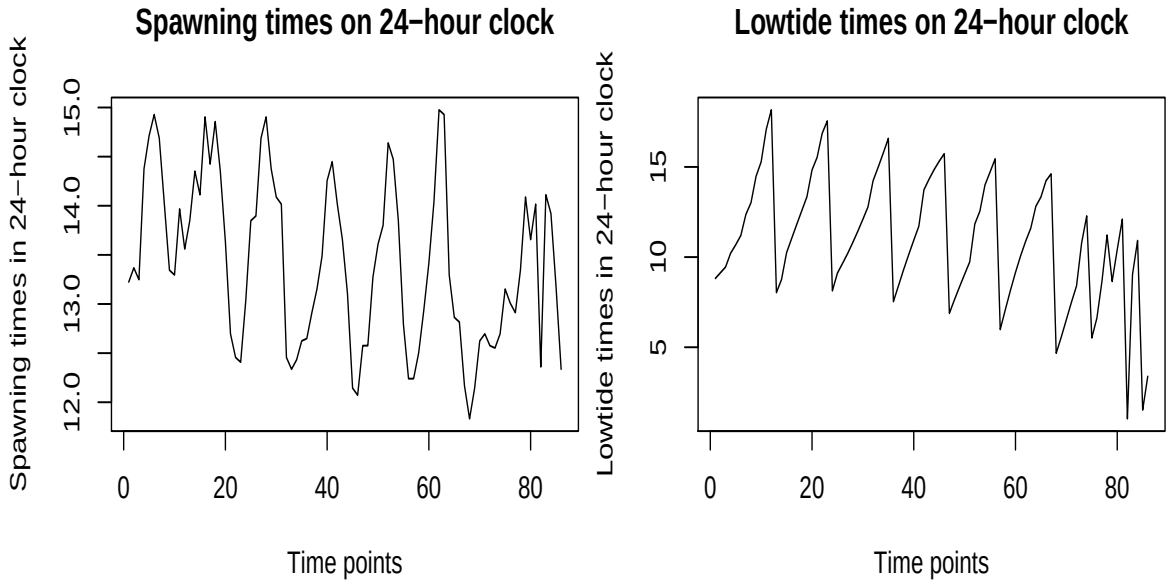

Figure 10: Plots of spawning times of a fish and low tide times on the 24-hour clock.

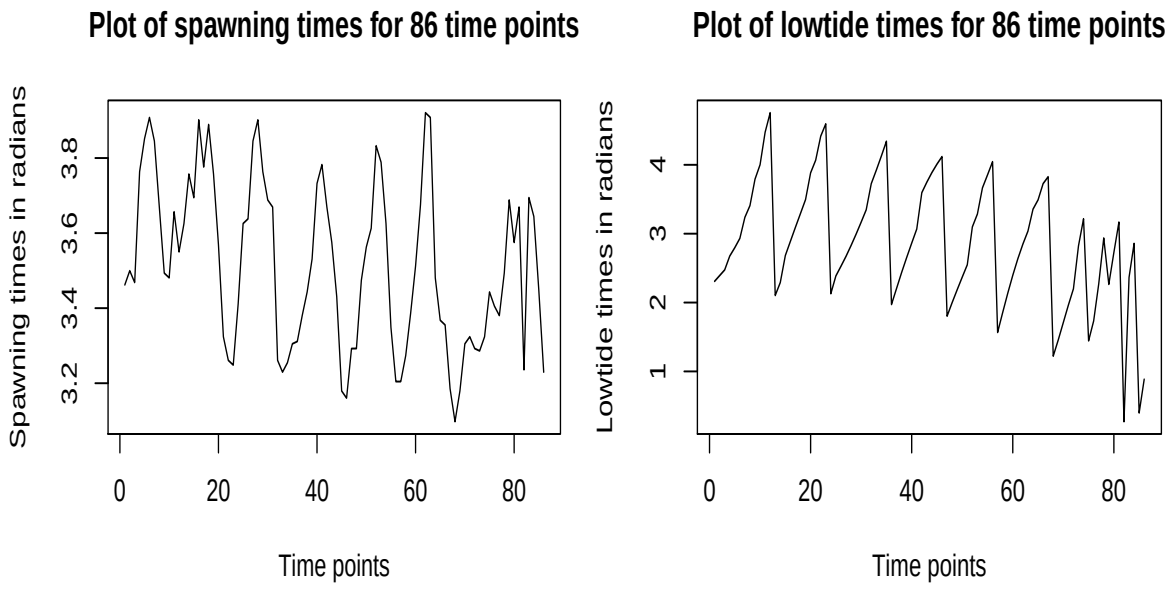

Figure 11: Plots of spawning times of a fish and low tide times after wrapping on $[0, 2\pi]$.

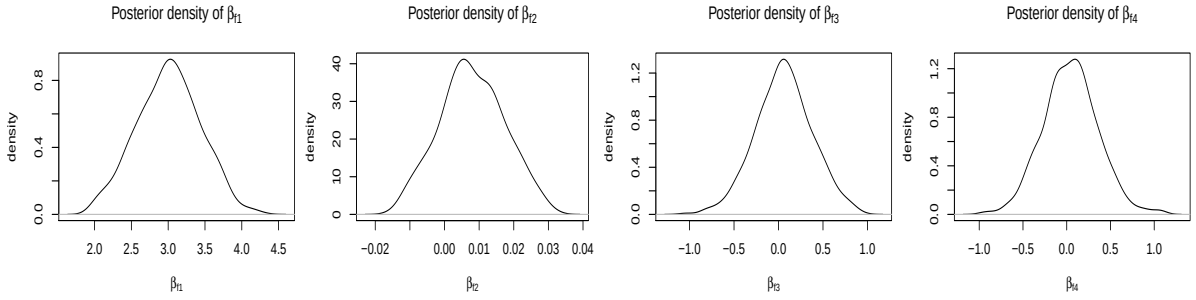

Figure 12: Posterior densities of the four components of $\boldsymbol{\beta}_f$ for the spawning time data.

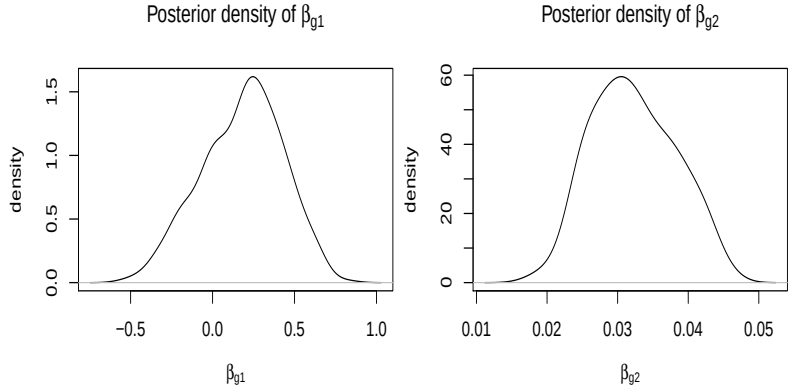

Figure 13: Posterior densities of the first two components of $\boldsymbol{\beta}_g$ for the spawning time data.

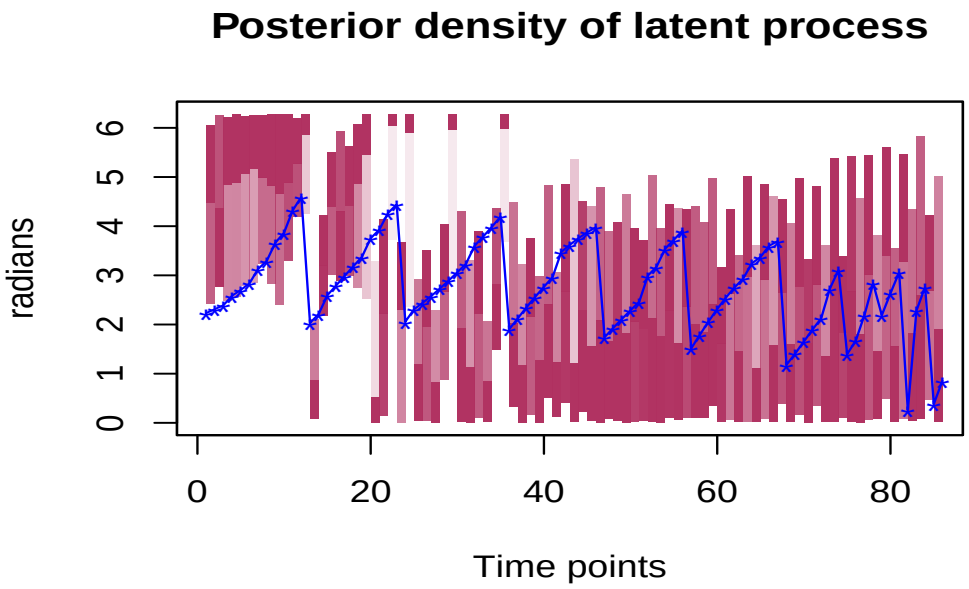

Figure 14: Representation of the marginal posterior densities of the latent variables corresponding to 85 low tide times as a color plot; progressively higher densities are represented by progressively intense colors. The blue stars represent the true low tide timings (in radians).

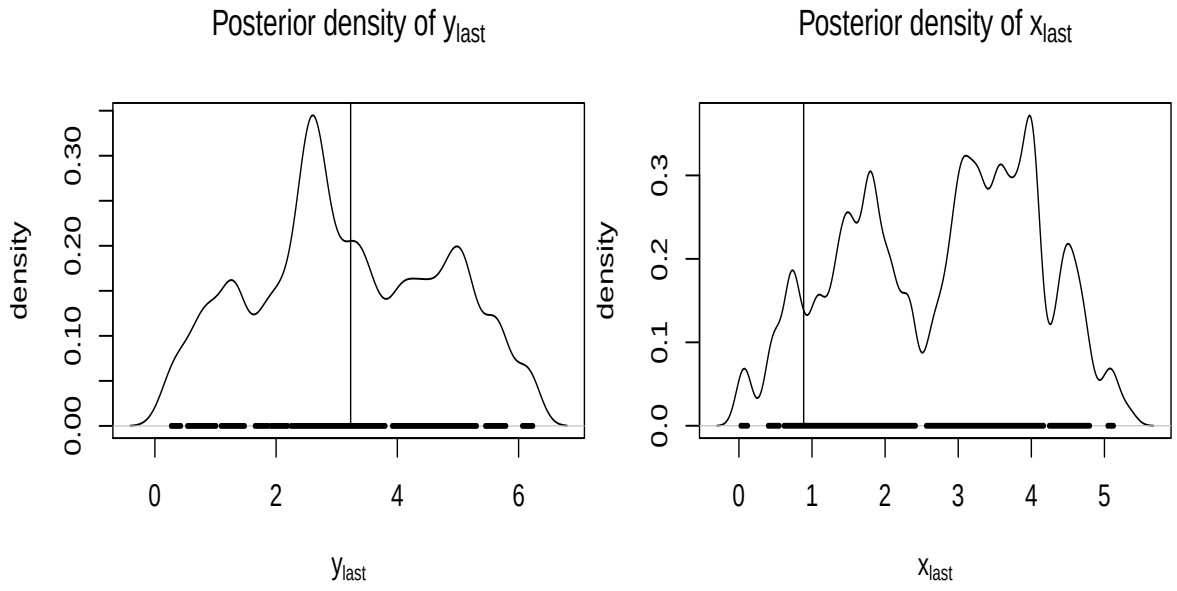

Figure 15: The left panel displays the posterior predictive density of the 86-th observation for the spawning time. The right panel depicts the posterior predictive density of the 86-th observation for low tide time. For both the plots, the thick horizontal line denotes the 95% highest posterior density credible interval and the vertical line denotes the true value (in radian).

6 Application to whale positional data

6.1 A brief description of the data set

An interesting data set on whale movement directions is available at http://nbviewer.jupyter.org/github/robertod
/earth_day_data_challenge/Analyzing%20whale%20tracks.ipynb, on which apply our model and methodologies to predict the directions of the ocean current.

Specifically, in this website 242 positions of a whale has been recorded in terms of latitudes and longitudes. The whale began its migration on 24th December of 2003 at the position 20.465 S, 40.04 W, and ended on 28th February of 2004 at 54.67 S, 26.261 W. This was an experimental project by Roberto De Almeida, who was interested whether whales could benefit from the ocean currents while migrating. For our purpose, first we processed the raw data by calculating the angles between these latitudes and longitudes, known as bearing, using the formula given in http://www.movable-type.co.uk/scripts/latlong.html. Finally, we obtained 241 circular univariate angular observations in radians. To reduce computational complexity here we have considered only the first 100 observations for our analysis setting aside the 101-th observation for the purpose of prediction. A plot of the first 101 bearings is shown in Figure 16. It is expected that the positions of the whale depends upon the directions of the ocean current, but the latter are not recorded. Hence, we anticipate that our general, nonparametric model and its corresponding methods will provide useful predictions of the direction of the ocean current, even though only the whale positions are observed.

6.2 Prior choices and MCMC implementation

The means of the prior distributions of $\boldsymbol{\beta}_f$ and $\boldsymbol{\beta}_g$ are set as $(5, 5, 5, 5)'$ and $(0, 2, 1, 1)'$, respectively, and their covariance matrices are as before considered to be the 4×4 identity matrix and the diagonal matrix with the diagonal entries as $(1, 1, 0, 0)'$. We made these choices to ensure adequate mixing of our MCMC chain. The MLEs of σ_f, σ_ϵ, σ_g and σ_η are found to be 1.15391, 0.24421, 0.19264 and 0.26019, respectively, using simulated annealing.

With these choices of prior parameters we implemented $2,50,000$ iterations of our MCMC algorithm, storing the last 50,000 observations for inference. The entire exercise took 25 hours 31 minutes in our server computer. The usual tests for convergence of MCMC indicated adequate mixing properties.

6.3 Results of whale positional data

We provide the plots of posterior densities of four components of $\boldsymbol{\beta}_f$ and two components of $\boldsymbol{\beta}_g$ in Figures 17 and 18, respectively. Figure 19 shows the marginal posterior distributions associated with the latent circular process depicted by progressively intense colors. In Figure 19, the blue stars indicate the posterior medians of the latent process. Finally, the posterior predictive densities corresponding to y_{101} and x_{101} are shown in Figure 20. The thin vertical line in the left panel denotes the true value of the 101-th observation of the bearing value and the thick, broken line on the horizontal axis represents the 95% highest density region of the posterior predictive density of y_{101}. As in our previous experiments, here also the true value falls well within the 95% highest posterior density credible interval. Thus, overall, the performance of our model and methods seems to be quite satisfactory.

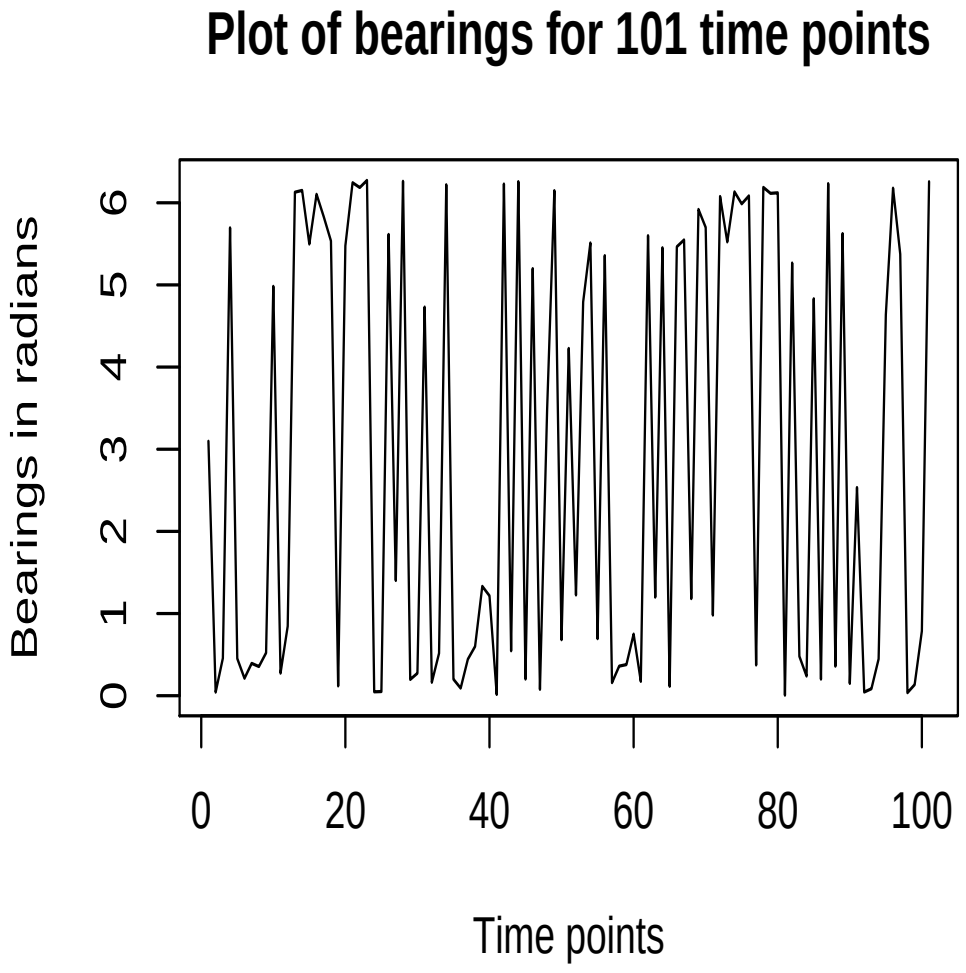

Figure 16: Plots of the bearings for 101 time points of the whale positions.

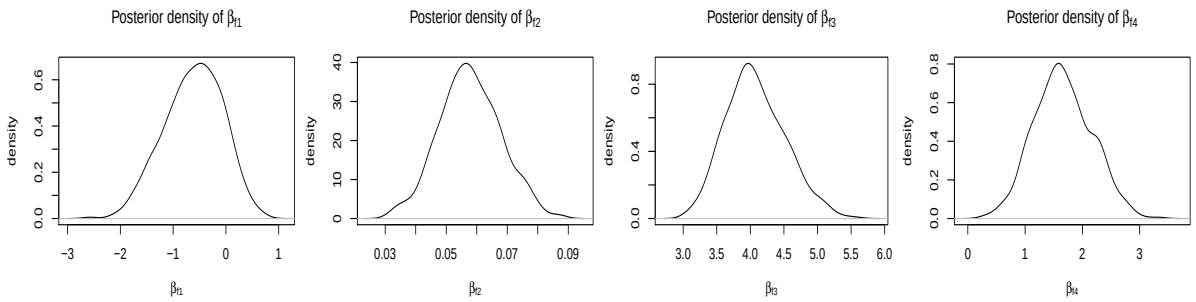

Figure 17: Posterior densities of the four components of $\boldsymbol{\beta}_f$ for the whale positional data.

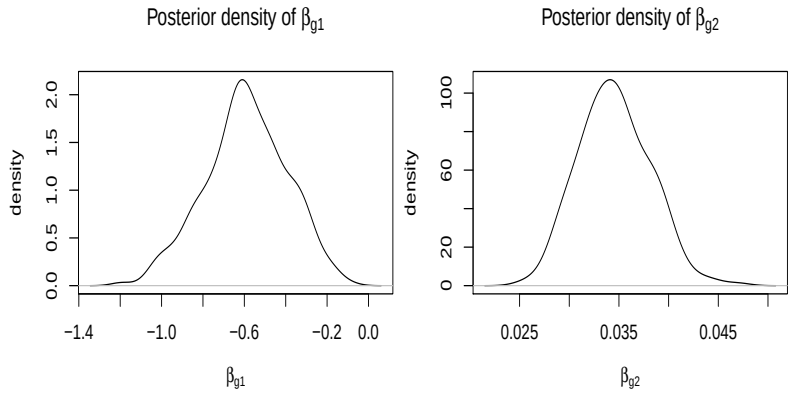

Figure 18: Posterior densities of the first two components of $\boldsymbol{\beta}_g$ for the whale positional data.

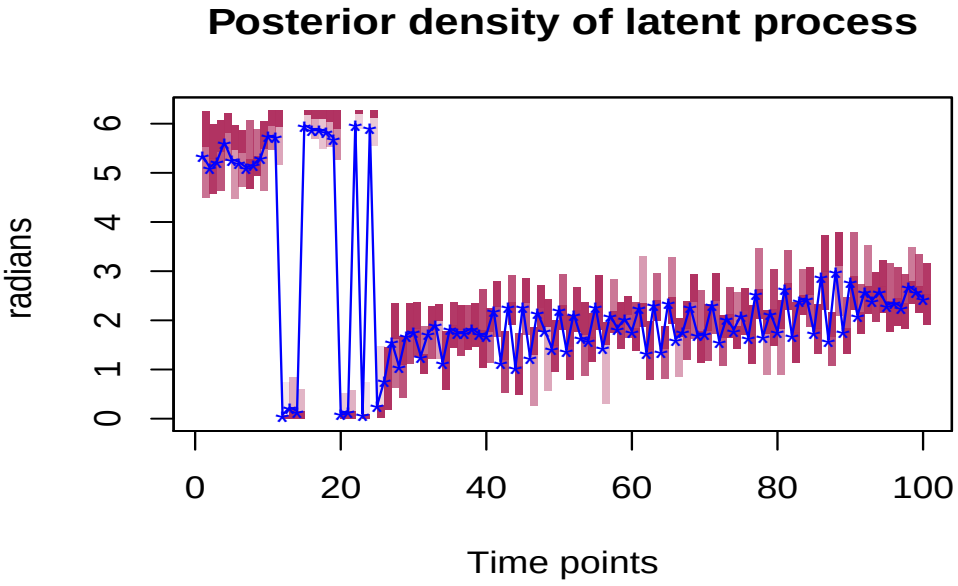

Figure 19: Depiction of the marginal posterior distributions of the latent variables using progressively intense colors for progressively higher densities. The blue stars represent the posterior medians of the latent process.

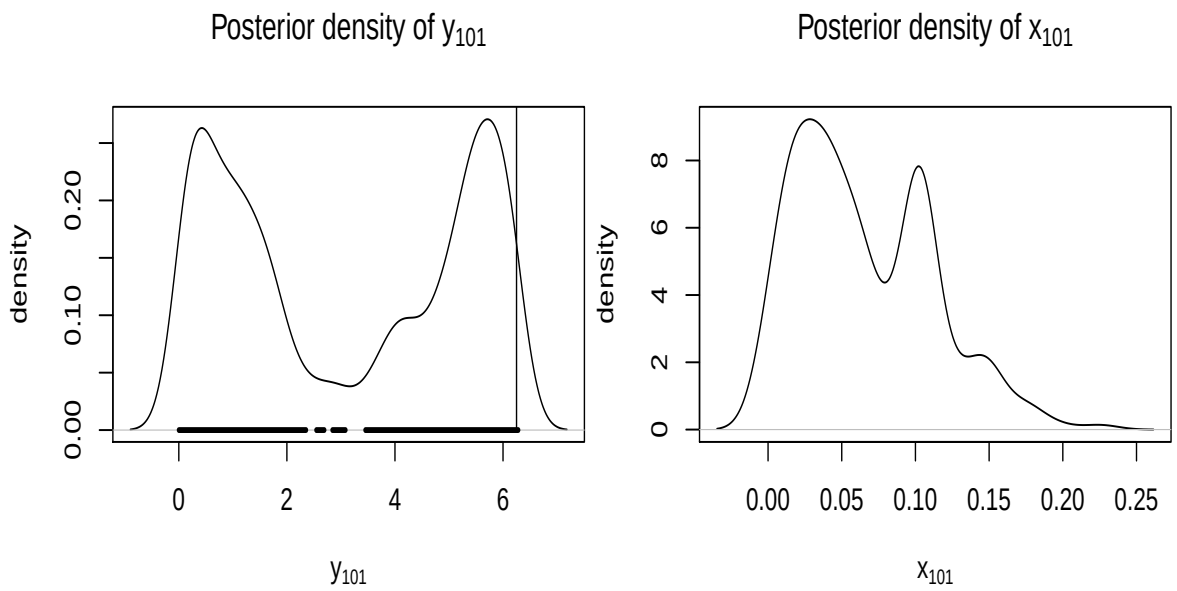

Figure 20: The left panel shows the posterior predictive density of the 101-th observation of bearing of the whale positional data. The thick horizontal line denotes the 95% highest posterior density credible interval and the vertical line denotes the true value. The right panel displays the posterior predictive density of the 101-th observation of direction of ocean current.

7 Discussion and conclusion

In nature there exist plentiful examples of circular time series where the underlying influential circular variable remains unrecorded. Some such examples, apart from the whale movement directions considered in this paper, are directions of flights of birds and missiles, where the underlying wind directions, although affects the flight directions, generally remains unrecorded. Modeling such circular time series using traditional parametric and nonparametric methods existing in the literature (for example, methods proposed in Breckling (1989), Fisher and Lee (1994), Holzmann *et al.* (2006), Hughes (2007), Marzio *et al.* (2012)) will be clearly far less effective compared to state space approaches that treat the underlying unrecorded process as a latent circular process. In this regard, we have introduced and developed a novel Bayesian nonparametric state space model for circular time series where the latent states also constitute a circular process.

Moreover, since it is clearly non-trivial to model general circular time series accounting for adequate non-Markov angular dependence structure, our endeavor seems to facilitate significant advance in this respect. Indeed, the observed time series in our state space model has a complex and realistic dependence structure, facilitated by the circular latent state process along with the structures induced by the wrapped Gaussian process, even though conditionally on the latent states and the observational function we assume the circular observations to be independent and further assume a Markovian structure of the latent states

conditional on the look-up table. These structures within our state space model facilitates an effective MCMC procedure, while ensuring highly realistic dependence structure. Such realistically complex dependence structures are absent in the traditional parametric and nonparametric circular time series models existing in the literature.

Other than our current work, the only research on state space models that considers circular latent states is that of Mazumder and Bhattacharya (2016a); however, they assume that the observed time series is associated with a linear process, unlike our observed circular time series. The observed circular process, as we argued, gave rise to significantly more complexities and difficult technical challenges in our case, compared to that of Mazumder and Bhattacharya (2016a). However, the complexities of our Bayesian model and methods notwithstanding, we have amply demonstrated with simulation studies as well as with three real data sets, the effectiveness of our proposed procedures.

Note that there perhaps exists a much larger class of circular time series in nature which depend upon unrecorded processes that are linear in nature, necessitating the development of Bayesian nonparametric state space models with observed circular process and latent linear process. But such development is a much simpler exercise given our current work and the developments provided in Ghosh *et al.* (2014). As more interesting alternatives, we shall focus on developing Bayesian nonparametric state space models and methods when the observed times series and the latent states are multivariate, with several linear and several circular components.

Acknowledgments

The authors are thankful to Professor Ulric Lund for providing the data on spawn timings and corresponding low tide timings. The authors are also thankful to the support staff of the website https://planetos.com/marinexplore/ for supplying the details of the whale positional data that is used in this paper.

References

Bhattacharya, S. (2007). A Simulation Approach to Bayesian Emulation of Complex Dynamic Computer Models. *Bayesian Analysis*, **2**, 783–816.

Bickel, J. P. and Doksum, A. K. (2007). *Mathematical Statistics*. Number 2nd Edition in Voume I. Pearson Prentice Hall.

Box, E. P. G. and Tiao, C. G. (1973). *Bayesian Inference in Statistical Analysis*. Addison Wesley Publishing Co.

Breckling, J. (1989). *The Analysis of Directional Time Series: Applications to Wind Speed and Direction*. Number 61 in Lecture Notes in Statistics. Springer-Verlag, Berlin.

Fisher, N. I. (1993). *Statistical Analysis of Circular Data*. Cambridge University Press, Cambridge.

Fisher, N. I. and Lee, A. J. (1994). Time Series Analysis of Circular Data. *Journal of the Royal Statistical Society. Series B*, **56**, 327–339.

Ghosh, A., Mukhopadhyay, S., Roy, S., and Bhattacharya, S. (2014). Bayesian Inference in Nonpaametric Dynamic State Space Models. *Statistical Methodology*, **21**, 35–48.

Holzmann, H., Munk, A., Suster, M., and Zucchini, W. (2006). Hidden Markov Models for Circular and Linear-Circular Time Series. *Environmental and Ecological Statistics*, **13**, 325–347.

Hughes, G. (2007). *Multivariate and Time Series Models for Circular Data with Applications to Protein Conformational Angles*. Doctoral thesis, University of Leeds.

Liu, J. (2001). *Monte Carlo Strategies in Scientific Computing*. Springer-Verlag, New York.

Lund, U. (1999). Least Circular Distance Regression for Directional Data. *Journal of Applied Statistics*, **26**, 723–733.

Marzio, M. D., Panzera, A., and Taylor, C. C. (2012). Non-parametric Smoothing and Prediction for Nonlinear Circular Time Series. *Journal of Time Series Analysis*, **33**, 620–630.

Mazumder, S. and Bhattacharya, S. (2016a). Bayesian Nonparametric Dynamic State-Space Modeling With Circular Latent States. *Journal of Statistical Theory and Practice*, **10**, 154–178.

Mazumder, S. and Bhattacharya, S. (2016b). Supplement to "Nonparametric Dynamic State-Space Modeling with Circular Latent and Observed States: A Bayesian Perspective". Submitted.

Ravindran, P. and Ghosh, S. (2011). Bayesian Analysis of Circular Data Using Wrapped Distributions. *Journal of Statistical Theory and Practice*, **4**, 1–20.

Robert, C. P. and Casella, G. (2004). *Monte Carlo Statistical Methods*. Springer-Verlag, New York.

Supplementary Material

S-1 Full conditional distributions of $\boldsymbol{\beta}_f$

$$
\begin{aligned}
[\boldsymbol{\beta}_f|\ldots] &\propto [\boldsymbol{\beta}_f][\boldsymbol{f}^*|x_1,\ldots,x_{T+1},\boldsymbol{\beta}_f,\sigma_f] \\
&\propto \exp\left\{-\frac{1}{2}(\boldsymbol{\beta}_f-\boldsymbol{\beta}_{f,0})'\Sigma^{-1}_{\boldsymbol{\beta}_{f,0}}(\boldsymbol{\beta}_f-\boldsymbol{\beta}_{f,0})-\frac{1}{2}(\boldsymbol{f}^*-H\boldsymbol{\beta}_f)'\sigma_f^{-2}A_f^{-1}(\boldsymbol{f}^*-H\boldsymbol{\beta}_f)\right\} \\
&\propto \exp\left\{-\frac{1}{2}\left[\boldsymbol{\beta}_f'\left(\Sigma^{-1}_{\boldsymbol{\beta}_{f,0}}+H'\sigma_f^{-2}A_f^{-1}H\right)\boldsymbol{\beta}_f-2\boldsymbol{\beta}_f'\left(\Sigma^{-1}_{\boldsymbol{\beta}_{f,0}}\boldsymbol{\beta}_{f,0}+H'\sigma_f^{-2}A_f^{-1}\boldsymbol{f}^*\right)\right]\right\}, \qquad (21)
\end{aligned}
$$

where $H=[\boldsymbol{h}'(1,x_1)\cdots\boldsymbol{h}'(T+1,x_{T+1})]'$. Therefore, the full conditional distribution of $\boldsymbol{\beta}_f$ is a four-variate normal distribution with mean

$$
E[\boldsymbol{\beta}_f|\ldots]=\left(\Sigma^{-1}_{\boldsymbol{\beta}_{f,0}}+H'\sigma_f^{-2}A_f^{-1}H\right)^{-1}\left(\Sigma^{-1}_{\boldsymbol{\beta}_{f,0}}\boldsymbol{\beta}_{f,0}+H'\sigma_f^{-2}A_f^{-1}\boldsymbol{f}^*\right) \qquad (22)
$$

and variance covariance matrix

$$
V[\boldsymbol{\beta}_f|\ldots]=\left(\Sigma^{-1}_{\boldsymbol{\beta}_{f,0}}+H'\sigma_f^{-2}A_f^{-1}H\right)^{-1}. \qquad (23)
$$

To update $\boldsymbol{\beta}_f$ we use Gibbs sampling.

S-2 Full conditional distribution of σ_f

$$
\begin{aligned}
[\sigma_f^2|\ldots] &\propto [\sigma_f^2][\boldsymbol{f}^*|x_1,\ldots,x_{T+1},\boldsymbol{\beta}_f,\sigma_f] \\
&= (\sigma_f^2)^{-\frac{\alpha_f+2+(T+1)}{2}}\exp\left\{-\frac{1}{2\sigma_f^2}\left[\gamma_f+(\boldsymbol{f}^*-H\boldsymbol{\beta}_f)'A_f^{-1}(\boldsymbol{f}^*-H\boldsymbol{\beta}_f)\right]\right\}. \qquad (24)
\end{aligned}
$$

Since A_f involves σ_f^2 (recall that $A_f=(\exp\left(-\sigma_f^4(i-j)^2\right)\cos(|x_i-x_j|))$ so, the closed form of the above posterior density is not tractable. Therefore, we use a random walk Metropolis-Hastings step to update σ_f^2.

S-3 Full conditional density of σ_ϵ

$$
\begin{aligned}
[\sigma_\epsilon^2] &\propto [\sigma_\epsilon^2] \prod_{t=1}^{T} [N_t | f^*(t, x_t), \sigma_\epsilon, x_t] \prod_{t=1}^{T} [y_t | N_t, f^*(t, x_t), \sigma_\epsilon, x_t] \\
&\propto (\sigma_\epsilon^2)^{-\frac{\alpha_\epsilon + 2 + T}{2}} \exp\left\{ -\frac{1}{2\sigma_\epsilon^2} \sum_{t=1}^{T} (y_t + 2\pi N_t - f^*(t, x_t))^2 \right\}. \qquad (25)
\end{aligned}
$$

Therefore, the full conditional distribution of σ_ϵ^2 is inverse gamma with the parameters $\frac{\alpha_\epsilon + T}{2}$ and $\frac{\sum_{t=1}^{T} (y_t + 2\pi N_t - f^*(t, x_t))^2}{2}$. Thus, we use the Gibbs sampling technique to update σ_ϵ^2.

S-4 Full conditional density of $\boldsymbol{f}^*_{D_T}$

$$
\begin{aligned}
[\boldsymbol{f}^*_{D_T} | \ldots] &\propto [\boldsymbol{f}^*_{D_T} | x_1, \ldots, x_{T+1}, \boldsymbol{\beta}_f, \sigma_f] \prod_{t=1}^{T} [N_t | f^*(t, x_t), \sigma_\epsilon, x_t] \prod_{t=1}^{T} [y_t | N_t, f^*(t, x_t), \sigma_\epsilon, x_t] \\
&\propto \exp\left\{ -\frac{1}{2} (\boldsymbol{f}^*_{D_T} - H_{D_T} \boldsymbol{\beta}_f)' \sigma_f^{-2} A^{-1}_{f, D_T} (\boldsymbol{f}^*_{D_T} - H_{D_T} \boldsymbol{\beta}_f) - \frac{1}{2\sigma_\epsilon^2} \sum_{t=1}^{T} (y_t + 2\pi N_t - f^*(t, x_t))^2 \right\} \\
&\propto \exp\left\{ -\frac{1}{2} \left[\boldsymbol{f}^*_{D_T} \left(\sigma_f^{-2} A^{-1}_{f, D_T} + \sigma_\epsilon^{-2} I_T \right) \boldsymbol{f}^*_{D_T} - 2 \boldsymbol{f}^*_{D_T} \left(\sigma_f^{-2} A^{-1}_{f, D_T} H_{D_T} \boldsymbol{\beta}_f + \sigma_\epsilon^{-2} [\boldsymbol{D}_T + 2\pi \boldsymbol{N}] \right) \right] \right\}, \qquad (26)
\end{aligned}
$$

where $\boldsymbol{D}_T + 2\pi \boldsymbol{N} = (y_1 + N_1, \ldots, y_T + N_T)'$. Hence, $[\boldsymbol{f}^*_{D_T} | \ldots]$ is a T-variate normal distribution with the parameters

$$
E[\boldsymbol{f}^*_{D_T} | \ldots] = \left(\sigma_f^{-2} A_f^{-1} + \sigma_\epsilon^{-2} I_T \right)^{-1} \left(\sigma_f^{-2} A^{-1}_{f, D_T} H_{D_T} \boldsymbol{\beta}_f + \sigma_\epsilon^{-2} [\boldsymbol{D}_T + 2\pi \boldsymbol{N}] \right) \qquad (27)
$$

and

$$
\operatorname{cov}[\boldsymbol{f}^*_{D_T} | \ldots] = \left(\sigma_f^{-2} A^{-1}_{f, D_T} + \sigma_\epsilon^{-2} I_T \right)^{-1}. \qquad (28)
$$

Hence, we use the Gibbs sampling technique to update $\boldsymbol{f}^*_{D_T}$.

S-5 Full conditional distribution of $f^*(T+1, x_{T+1})$

$$
[f^*(T+1, x_{T+1}) | \ldots] \propto [f^*(T+1, x_{T+1}) | \boldsymbol{f}^*_{D_T}, x_{T+1}, \boldsymbol{\beta}_f, \sigma_f]. \qquad (29)
$$

Hence, $[f^*(T+1, x_{T+1})|\ldots]$ follows the univariate normal distribution with parameters $\mu_{f^*(T+1,\, x_{T+1})}$ and variance $\sigma^2_{f^*(T+1,\, x_{T+1})}$, and so, we update $f^*(T+1, x_{T+1})$ by Gibbs sampling.

S-6 Full conditional density of N_t, $t = 1, \ldots, T$

$$
\begin{aligned}
[N_t|\ldots] &\propto [N_t|f^*(t, x_t), \sigma_\epsilon, x_t][y_t|N_t, f^*(t, x_t), \sigma_\epsilon, x_t] \\
&\propto \exp\left(-\frac{1}{2\sigma^2_\epsilon}(y_t + 2\pi N_t - f^*(t, x_t))^2\right) I_{\{\ldots,-1,0,1,\ldots\}}(N_t),\ t = 1, \ldots, T. \qquad (30)
\end{aligned}
$$

The full conditional distribution of N_t, $t = 1, \ldots, T$, are not tractable, and so we update them by random walk Metropolis-Hastings steps.

S-7 Full conditional density of $\boldsymbol{\beta}_g$

$$
\begin{aligned}
[\boldsymbol{\beta}_g|\cdots] \propto [\boldsymbol{\beta}_g][\boldsymbol{D}_z, g^*(1, x_0)|x_0, \boldsymbol{\beta}_g, \sigma^2_g] \prod_{t=2}^{T+1} [x_t|\boldsymbol{\beta}_g, \sigma^2_\eta, \sigma^2_g, \boldsymbol{D}_z, x_{t-1}, K_t] \prod_{t=2}^{T+1} \big[K_t|\boldsymbol{\beta}_g, \sigma^2_\eta \\
\sigma^2_g, \boldsymbol{D}_z, x_{t-1}\big] \qquad (31)
\end{aligned}
$$

We write down the right hand side of (31) as follows:

$$
\begin{aligned}
&[\boldsymbol{\beta}_g][\boldsymbol{D}_z, g^*(1, x_0)|x_0, \boldsymbol{\beta}_g] \prod_{t=2}^{T+1} [x_t|\boldsymbol{\beta}_g, \sigma^2_\eta, \boldsymbol{D}_z, x_{t-1}, K_t] \prod_{t=2}^{T+1} [K_t|\boldsymbol{\beta}_g, \sigma^2_\eta, \boldsymbol{D}_z, x_{t-1}] \\
&\propto \exp\left(-\frac{1}{2}(\boldsymbol{\beta}_g - \boldsymbol{\beta}_{g,0})' \boldsymbol{\Sigma}^{-1}_{\beta_g,0} (\boldsymbol{\beta}_g - \boldsymbol{\beta}_{g,0})\right) \\
&\times \exp\left(-\frac{1}{2}[(\boldsymbol{D}_z, g^*)' - (\boldsymbol{H}_{D_z}\boldsymbol{\beta}_g, \boldsymbol{h}'(1, x_0))']' \boldsymbol{A}^{-1}_{D_z, g^*(1,x_0)} [(\boldsymbol{D}_z, g^*)' - (\boldsymbol{H}_{D_z}\boldsymbol{\beta}_g, \boldsymbol{h}'(1, x_0))']\right) \\
&\quad \times \exp\left\{-\sum_{i=2}^{T+1} \frac{1}{2\sigma^2_{x_t}} (x_t + 2\pi K_t - \mu_{x_t})^2\right\} \prod_{t=2}^{T+1} I_{[0,2\pi]}(x_t). \qquad (32)
\end{aligned}
$$

Observe that the denominator of $[x_t|\boldsymbol{\beta}_g, \sigma^2_\eta, \boldsymbol{D}_z, x_{t-1}, K_t]$ cancels with the density of $[K_t|\boldsymbol{\beta}_g, \sigma^2_\eta, \boldsymbol{D}_z, x_{t-1}]$, for each $t = 2, \ldots, T+1$. Also, we note that the indicator function does not involve $\boldsymbol{\beta}_g$ for any $t = 2, \ldots, T+1$. Therefore, after simplifying the exponent terms and ignoring the indicator

function we can write

$$[\boldsymbol{\beta}_g|\cdots] \propto \exp\left\{-\frac{1}{2}(\boldsymbol{\beta}_g - \mu_{\beta_g})'\boldsymbol{\Sigma}_{\beta_g}^{-1}(\boldsymbol{\beta}_g - \mu_{\beta_g})\right\}, \tag{33}$$

where

$$\begin{aligned}
\mu_{\beta_g} = E[\boldsymbol{\beta}_g|\cdots] = \Bigg\{ & \boldsymbol{\Sigma}_{\beta_g,0}^{-1} + \frac{1}{\sigma_g^2}[\boldsymbol{H}'_{D_z}, \boldsymbol{h}(1,x_0)]\boldsymbol{A}_{D_z,g^*(1,x_0)}^{-1}[\boldsymbol{H}'_{D_z}, \boldsymbol{h}(1,x_0)]' \\
& + \sum_{t=1}^{T} \frac{\left(\boldsymbol{H}'_{D_z}\boldsymbol{A}_{g,D_z}^{-1}\boldsymbol{s}_{g,D_z}(t+1,x_t) - \boldsymbol{h}(t+1,x_t)\right)\left(\boldsymbol{H}'_{D_z}\boldsymbol{A}_{g,D_z}^{-1}\boldsymbol{s}_{g,D_z}(t+1,x_t) - \boldsymbol{h}(t+1,x_t)\right)'}{\sigma_{x_t}^2} \Bigg\}^{-1} \\
& \Bigg\{ \boldsymbol{\Sigma}_{\beta_g,0}^{-1}\boldsymbol{\beta}_{g,0} + \frac{1}{\sigma_g^2}[\boldsymbol{H}'_{D_z}, \boldsymbol{h}(1,x_0)]\boldsymbol{A}_{D_z,g^*(1,x_0)}^{-1}[\boldsymbol{D}_z, g^*(1,x_0)] \\
& + \sum_{t=1}^{T} \frac{\left(x_{t+1} + 2\pi K_{t+1} - \boldsymbol{s}_{g,D_z}(t+1,x_t)'\boldsymbol{A}_{g,D_z}^{-1}\boldsymbol{D}_z\right)\left(\boldsymbol{h}(t+1,x_t) - \boldsymbol{H}'_{D_z}\boldsymbol{A}_{g,D_z}^{-1}\boldsymbol{s}_{g,D_z}(t+1,x_t)\right)}{\sigma_{x_t}^2} \Bigg\}
\end{aligned} \tag{34}$$

and

$$\begin{aligned}
\boldsymbol{\Sigma}_{\beta_g} = V[\boldsymbol{\beta}_g|\cdots] = \Bigg\{ & \boldsymbol{\Sigma}_{\beta_g,0}^{-1} + \frac{1}{\sigma_g^2}[\boldsymbol{H}'_{D_z}, \boldsymbol{h}(1,x_0)]\boldsymbol{A}_{D_z,g^*(1,x_0)}^{-1}[\boldsymbol{H}'_{D_z}, \boldsymbol{h}(1,x_0)]' \\
& + \sum_{t=1}^{T} \frac{\left(\boldsymbol{H}'_{D_z}\boldsymbol{A}_{g,D_z}^{-1}\boldsymbol{s}_{g,D_z}(t+1,x_t) - \boldsymbol{h}(t+1,x_t)\right)\left(\boldsymbol{H}'_{D_z}\boldsymbol{A}_{g,D_z}^{-1}\boldsymbol{s}_{g,D_z}(t+1,x_t) - \boldsymbol{h}(t+1,x_t)\right)'}{\sigma_{x_t}^2} \Bigg\}^{-1}.
\end{aligned} \tag{35}$$

Hence $[\boldsymbol{\beta}_g|\cdots]$ follows a four-variate normal distribution with mean and variance μ_{β_g} and $\boldsymbol{\Sigma}_{\beta_g}$, respectively. Therefore, we update $\boldsymbol{\beta}_g$ by Gibbs sampling.

S-8 Full conditional density of σ_η^2

$$\begin{aligned}
[\sigma_\eta^2|\cdots] &\propto [\sigma_\eta^2][x_1|g^*(1,x_0),\sigma_\eta^2,K_1][K_1|g^*(1,x_0),\sigma_\eta^2]\prod_{t=2}^{T+1}[x_t|\boldsymbol{\beta}_g,\sigma_\eta^2,\sigma_g^2,\boldsymbol{D}_z,x_{t-1},K_t] \\
&\quad \times \prod_{t=2}^{T+1}[K_t|\boldsymbol{\beta}_g,\sigma_g^2,\sigma_\eta^2,\boldsymbol{D}_z,x_{t-1}] \\
&\propto [\sigma_\eta^2]\exp\left\{-\sum_{i=2}^{T+1}\frac{1}{2\sigma_{x_t}^2}(x_t + 2\pi K_t - \mu_{x_t})^2\right\}\exp\left\{-\frac{1}{2\sigma_\eta^2}(x_1 + 2\pi K_1 - g^*)^2\right\}.
\end{aligned} \tag{36}$$

The right hand side of (36) does not have a closed form and hence we update σ_η^2 using a random walk Metropolis-Hastings step.

S-9 Full conditional density of σ_g^2

$$[\sigma_g^2|\cdots] \propto [\sigma_g^2][\boldsymbol{D}_z, g^*(1,x_0)|x_0,\boldsymbol{\beta}_g,\sigma_g^2]\prod_{t=2}^{T+1}[x_t|\boldsymbol{\beta}_g,\sigma_\eta^2,\sigma_g^2,\boldsymbol{D}_z,x_{t-1},K_t]\prod_{t=2}^{T+1}\left[K_t|\boldsymbol{\beta}_g,\sigma_g^2,\right.$$
$$\left.\sigma_\eta^2,\boldsymbol{D}_z,x_{t-1}\right]. \tag{37}$$

It is not possible to obtain a closed form of the right hand side of above equation and therefore, to update σ_g^2, we consider a random walk Metropolis-Hastings step.

S-10 Full conditional distribution of x_0

$$[x_0|\cdots] \propto [x_0][\boldsymbol{D}_z, g^*(1,x_0)|x_0,\boldsymbol{\beta}_g,\sigma_g^2]. \tag{38}$$

The closed form of right hand side of (38) is not available. So, we update x_0 using a random walk Metropolis-Hastings step.

S-11 Full conditional density of $g^*(1,x_0)$

$$\begin{aligned}[g^*(1,x_0)|\cdots] &\propto [g^*(1,x_0)|x_0,\boldsymbol{\beta}_g,\sigma_g^2][\boldsymbol{D}_z|g^*(1,x_0),x_0,\boldsymbol{\beta}_g,\sigma_g^2][x_1|g^*(1,x_0),x_0,\sigma_\eta^2,K_1]\\ &\quad\times[K_1|g^*(1,x_0),\sigma_\eta^2]\\ &\propto [g^*(1,x_0)|x_0,\boldsymbol{\beta}_g][\boldsymbol{D}_z|g^*(1,x_0),x_0,\boldsymbol{\beta}_g]\exp\left\{-\frac{1}{2\sigma_\eta^2}(x_1+2\pi K_1-g^*)^2\right\}\\ &\propto \exp\left\{-\frac{1}{2\gamma_g^2}(g^*-\nu_g)^2\right\},\end{aligned} \tag{39}$$

where

$$\begin{aligned}\nu_g = E[g^*(1,x_0)|\cdots] &= \left\{\frac{1}{\sigma_\eta^2}+\frac{1}{\sigma_g^2}(1+\boldsymbol{s}_{g,D_z}(1,x_0)'\boldsymbol{\Sigma}_{g,D_z}^{-1}\boldsymbol{s}_{g,D_z}(1,x_0))\right\}^{-1}\\ &\quad\left\{\frac{x_1+2\pi K_1}{\sigma_\eta^2}+\frac{1}{\sigma_g^2}(\boldsymbol{h}(1,x_0)'\boldsymbol{\beta}_g+\boldsymbol{s}'_{g,D_z}\boldsymbol{\Sigma}_{g,D_z}^{-1}\boldsymbol{D}_z^*)\right\}\end{aligned} \tag{40}$$

and

$$\gamma_g^2 = V[g^*(1,x_0)|\cdots] = \left\{\frac{1}{\sigma_\eta^2} + \frac{1}{\sigma_g^2}(1 + \boldsymbol{s}_{g,D_z}(1,x_0)'\boldsymbol{\Sigma}_{g,D_z}^{-1}\boldsymbol{s}_{g,D_z}(1,x_0))\right\}^{-1}, \tag{41}$$

with

$$\boldsymbol{D}_z^* = \boldsymbol{D}_z - \boldsymbol{H}_{D_z}\boldsymbol{\beta}_g + \boldsymbol{h}(1,x_0)'\boldsymbol{\beta}_g\boldsymbol{s}_{g,D_z}, \tag{42}$$

and

$$\boldsymbol{\Sigma}_{g,D_z} = \boldsymbol{A}_{g,D_z} - \boldsymbol{s}_{g,D_z}(1,x_0)\boldsymbol{s}_{g,D_z}(1,x_0)'. \tag{43}$$

Hence $[g^*|\cdots]$ follows a univariate normal distribution with mean ν_g and variance γ_g. Thus, we update g^* using Gibbs sampling.

S-12 Full conditional of $\boldsymbol{D}_z$

$$[\boldsymbol{D}_z|\cdots] \propto [\boldsymbol{D}_z|g^*(1,x_0),x_0,\boldsymbol{\beta}_g,\sigma_g^2]\prod_{t=2}^{T+1}[x_t|\boldsymbol{\beta}_g,\sigma_g^2,\sigma_\eta^2,\boldsymbol{D}_z,x_{t-1},K_t]\prod_{t=2}^{T+1}[K_t|\boldsymbol{\beta}_g,\sigma_g^2,\sigma_\eta^2,\boldsymbol{D}_z,x_{t-1}] \tag{44}$$

After simplification it turns out that the full conditional distribution of $\boldsymbol{D}_z$ is an n-variate normal with mean

$$\begin{aligned} E(\boldsymbol{D}_z|\cdots) = &\left\{\frac{\boldsymbol{\Sigma}_{g,D_z}^{-1}}{\sigma_g^2} + \boldsymbol{A}_{g,D_z}^{-1}\left(\sum_{t=1}^{T}\frac{s_{g,D_z}(t+1,x_t)s_{g,D_z}'(t+1,x_t)}{\sigma_{x_t}^2}\right)\boldsymbol{A}_{g,D_z}^{-1}\right\}^{-1} \\ &\times\left\{\frac{\boldsymbol{\Sigma}_{g,D_z}^{-1}\boldsymbol{\mu}_{g,D_z}}{\sigma_g^2} + \boldsymbol{A}_{g,D_z}^{-1}\right. \\ &\left.\sum_{t=1}^{T}\frac{s_{g,D_z}(t+1,x_t)\{x_{t+1}+2\pi K_{t+1} - \boldsymbol{\beta}_g'(\boldsymbol{h}(1,t+1,x_t) - \boldsymbol{H}_{D_z}'\boldsymbol{A}_{g,D_z}^{-1}s_{g,D_z}(t+1,x_t))\}}{\sigma_{x_t^2}}\right\} \end{aligned} \tag{45}$$

and covariance matrix

$$V(\boldsymbol{D}_z|\cdots) = \left\{\frac{\boldsymbol{\Sigma}_{g,D_z}^{-1}}{\sigma_g^2} + \boldsymbol{A}_{g,D_z}^{-1}\left(\sum_{t=1}^{T}\frac{s_{g,D_z}(t+1,x_t)s_{g,D_z}'(t+1,x_t)}{\sigma_{x_t}^2}\right)\boldsymbol{A}_{g,D_z}^{-1}\right\}^{-1}, \tag{46}$$

where $\sigma_{x_t}^2 = \sigma_\eta^2 + \sigma_g^2\left(1 - (\boldsymbol{s}_{g,D_z}(t,x_{t-1}))'\boldsymbol{A}_{g,D_z}^{-1}\boldsymbol{s}_{g,D_z}(t,x_{t-1})\right)$, for $t = 1,\ldots,T$. We update $\boldsymbol{D}_z$ using the

Gibbs sampling technique.

S-13 Full conditional of x_1

$$
\begin{aligned}
[x_1|\cdots] \propto\ & [x_1|g^*(1,x_0),\sigma_\eta^2][\boldsymbol{f}^*_{D_T}|x_1,\ldots,x_T,\boldsymbol{\beta}_f,\sigma_f][N_1|f^*(1,x_1),\sigma_\epsilon,x_1] \\
& [y_1|N_1,f^*(1,x_1),\sigma_\epsilon,x_1][x_2|\boldsymbol{\beta}_g,\sigma_g^2,\sigma_\eta^2,\boldsymbol{D}_z,x_1,K_2][K_2|\boldsymbol{\beta}_g,\sigma_g^2,\sigma_\eta^2,\boldsymbol{D}_z,x_1] \\
\propto\ & \frac{1}{\sqrt{2\pi}\sigma_\eta}\exp\left(-\frac{1}{2\sigma_\eta^2}(x_1+2\pi K_1-g^*)^2\right) I_{[0,2\pi]}(x_1) \\
& \times\exp\left\{-\frac{1}{2}(\boldsymbol{f}^*_{D_T}-H_{D_T}\boldsymbol{\beta}_f)'\sigma_f^{-2}A^{-1}_{f,D_T}(\boldsymbol{f}^*_{D_T}-H_{D_T}\boldsymbol{\beta}_f)-\frac{1}{2\sigma_\epsilon^2}(y_1+2\pi N_1-f^*(1,x_1))^2\right\} \\
& \times\frac{1}{\sqrt{2\pi}\sigma_{x_2}}\exp\left(-\frac{1}{2\sigma_{x_2}^2}(x_2+2\pi K_2-\mu_{x_2})^2\right), \qquad (47)
\end{aligned}
$$

where $\mu_{x_2}=\boldsymbol{h}(2,x_1)'\boldsymbol{\beta}_g+\boldsymbol{s}_{g,D_z}((2,x_1))'\boldsymbol{A}^{-1}_{g,D_z}(\boldsymbol{D}_z-\boldsymbol{H}_{D_z}\boldsymbol{\beta}_g)$ and

$\sigma^2_{x_2}=\sigma^2_\eta+\sigma^2_g\left(1-(\boldsymbol{s}_{g,D_z}(2,x_1))'\boldsymbol{A}^{-1}_{g,D_z}\boldsymbol{s}_{g,D_z}(2,x_1)\right)$. However, the closed form of the above expression is not tractable. So, we update x_1 with a random walk Metropolis-Hastings step.

S-14 Full conditional of x_{t+1}, for $t=1,\ldots,T-1$

$$
\begin{aligned}
[x_{t+1}|\cdots] \propto\ & [x_{t+1}|\boldsymbol{\beta}_g,\sigma_g^2,\sigma_\eta^2,\boldsymbol{D}_z,x_t][x_{t+2}|\boldsymbol{\beta}_g,\sigma_g^2,\sigma_\eta^2,\boldsymbol{D}_z,x_{t+1},K_{t+2}]\left[K_{t+2}|\boldsymbol{\beta}_g,\sigma_g^2,\sigma_\eta^2,\right. \\
& \left.\boldsymbol{D}_z,x_{t+1}\right][\boldsymbol{f}^*_{D_T}|x_1,\ldots,x_T,\boldsymbol{\beta}_f,\sigma_f][N_{t+1}|f^*(t+1,x_{t+1}),\sigma_\epsilon,x_{t+1}] \\
& \times[y_{t+1}|N_{t+1},f^*(t+1,x_{t+1}),\sigma_\epsilon,x_{t+1}] \\
\propto\ & \frac{1}{\sqrt{2\pi}\sigma_{x_{t+1}}}\exp\left(-\frac{1}{2\sigma^2_{x_{t+1}}}(x_{t+1}+2\pi K_{t+1}-\mu_{x_{t+1}})^2\right) I_{[0,2\pi]}(x_{t+1}) \\
& \times\frac{1}{\sqrt{2\pi}\sigma_{x_{t+2}}}\exp\left(-\frac{1}{2\sigma^2_{x_{t+2}}}(x_{t+2}+2\pi K_{t+2}-\mu_{x_{t+2}})^2\right) \\
& \times\exp\left\{-\frac{1}{2}(\boldsymbol{f}^*_{D_T}-H_{D_T}\boldsymbol{\beta}_f)'\sigma_f^{-2}A^{-1}_{f,D_T}(\boldsymbol{f}^*_{D_T}-H_{D_T}\boldsymbol{\beta}_f)-\right. \\
& \left.\frac{1}{2\sigma_\epsilon^2}(y_{t+1}+2\pi N_{t+1}-f^*(t+1,x_{t+1}))^2\right\} \qquad (48)
\end{aligned}
$$

The expression of the full conditional distribution of x_{t+1}, $t=1,\ldots T-1$, are not tractable and therefore, we update x_{t+1}, $t=1,\ldots T-1$, using random walk Metropolis-Hastings steps.

S-15 Full conditional of x_{T+1}

$$
\begin{aligned}
[x_{T+1}|\cdots] &\propto [x_{T+1}|\boldsymbol{\beta}_g, \sigma_g^2, \sigma_\eta^2, \boldsymbol{D}_z, x_T, K_{T+1}][f^*(T+1, x_{T+1})|\boldsymbol{f}^*_{D_T}, x_{T+1}, \boldsymbol{\beta}_f, \sigma_f] \\
&\propto \frac{\frac{1}{\sqrt{2\pi}\sigma_{x_{T+1}}} \exp\left(-\frac{1}{2\sigma^2_{x_{T+1}}}(x_{T+1} + 2\pi K_{T+1} - \mu_{x_{T+1}})^2\right) I_{[0,2\pi]}(x_{T+1})}{\Phi\left(\frac{2\pi(K_{T+1}+1)-\mu_{x_{T+1}}}{\sigma_{x_{T+1}}}\right) - \Phi\left(\frac{2\pi K_{T+1}-\mu_{x_{T+1}}}{\sigma_{x_{T+1}}}\right)} \\
&\quad \times \frac{1}{\sqrt{2\pi}\sigma_{f^*(T+1, x_{T+1})}} \exp\left(-\frac{1}{2\sigma^2_{f^*(T+1, x_{T+1})}}(f^*(T+1, x_{T+1}) - \mu_{f^*(T+1, x_{T+1})})^2\right) \\
&\propto \exp\left(-\frac{1}{2\sigma^2_{x_{T+1}}}(x_{T+1} + 2\pi K_{T+1} - \mu_{x_{T+1}})^2\right) I_{[0,2\pi]}(x_{T+1}) \\
&\quad \times \frac{1}{\sqrt{2\pi}\sigma_{f^*(T+1, x_{T+1})}} \exp\left(-\frac{1}{2\sigma^2_{f^*(T+1, x_{T+1})}}(f^*(T+1, x_{T+1}) - \mu_{f^*(T+1, x_{T+1})})^2\right). \qquad (49)
\end{aligned}
$$

We note that $\mu_{x_{T+1}}$ and $\sigma^2_{x_{T+1}}$ do not depend upon x_{T+1} but $\mu_{f^*(T+1, x_{T+1})}$ and $\sigma_{f^*(T+1, x_{T+1})}$ do depend upon x_{T+1}. However, in any case the right hand side of the above equation is not tractable. Therefore, we update x_{T+1} as well using a random walk Metropolis-Hastings step.

S-16 Full conditional density of K_1

$$
\begin{aligned}
[K_1|\cdots] &\propto [K_1|g^*(1, x_0), \sigma_\eta^2][x_1|g^*(1, x_0), \boldsymbol{\beta}_g, \sigma_\eta^2, K_1] \\
&\propto \frac{1}{\sqrt{2\pi}\sigma_\eta} \exp\left(-\frac{1}{2\sigma_\eta^2}(x_1 + 2\pi K_1 - g^*)^2\right) I_{\{\ldots,-1,0,1,\ldots\}}(K_1). \qquad (50)
\end{aligned}
$$

The full conditional distribution of K_1 is not tractable and hence we update K_1 using a random walk Metropolis-Hastings step.

S-17 Full conditional density of K_t

$$
\begin{aligned}
[K_t|\cdots] &\propto [x_t|\boldsymbol{\beta}_g, \sigma_\eta^2, \boldsymbol{D}_z, x_{t-1}, K_t][K_t|\boldsymbol{\beta}_g, \sigma_\eta^2, \boldsymbol{D}_z, x_{t-1}], \\
&\propto \exp\left(-\frac{1}{2\sigma^2_{x_t}}(x_t + 2\pi K_t - \mu_{x_t})^2\right) I_{\{\ldots,-1,0,1,\ldots\}}(K_t),\ t = 2, \ldots, T+1. \qquad (51)
\end{aligned}
$$

As in the case of K_1, here also closed forms of the full conditional distributions of K_t, $t = 2, \ldots, T+1$ are not available, and hence we update K_t, $t = 2, \ldots, T+1$, using random walk Metropolis-Hastings steps.